DOI:10.1093/jnci/djs232
Advance Access publication on May 25, 2012.

ARTICLE

Effect of ADAM28 on Carcinoma Cell Metastasis by Cleavage of von Willebrand Factor

Satsuki Mochizuki, Kenji Soejima, Masayuki Shimoda, Hitoshi Abe, Aya Sasaki, Hirotaka James Okano, Hideyuki Okano, Yasunori Okada

Manuscript received September 2, 2011; revised April 4, 2012; accepted April 6, 2012.

Correspondence to: Yasunori Okada, MD, PhD, Department of Pathology, School of Medicine, Keio University, 35 Shinanomachi, Shinjuku-ku, Tokyo 160-0016, Japan (e-mail: okada@z6.keio.jp).

Background A disintegrin and metalloproteinase 28 (ADAM28) is implicated in tumor growth and metastasis in human breast and non–small cell lung carcinomas. We explored the mechanism of ADAM28-mediated metastasis by searching for new substrates of ADAM28.

Methods We used a yeast two-hybrid system to screen the human lung cDNA library for ADAM28-binding proteins and identified von Willebrand factor (VWF) as a potential candidate. Binding was confirmed using yeast two-hybrid and protein binding assays, and ADAM28-mediated cleavage of VWF was analyzed by immunoblotting. Exogenous VWF-induced apoptosis in vitro was examined in human lung carcinoma (PC-9 and Calu-3), breast carcinoma (MDA-MB231 and MCF-7), renal cell carcinoma (Caki-2 and 769P), and hepatocellular carcinoma (HepG2) cells, and expression of ADAM28 was assessed by reverse transcription–polymerase chain reaction and immunoblotting. Effect on lung metastasis of PC-9 and MDA-MB231 cells was assessed by knockdown of ADAM28 expression using short hairpin RNAs (ADAM28-shRNA) and small interfering RNAs (ADAM28-siRNA), and inhibition of activity using neutralizing anti-ADAM28 antibody, in a mouse xenograft model by in vivo imaging (n = 9 mice per group). All statistical tests were two-sided.

Results ADAM28 could bind to and cleave native VWF. Cells with very low ADAM28 expression (MCF-7, 769P, and HepG2) were susceptible to VWF-induced apoptosis, whereas cells with high expression (PC-9, Calu-3, MDA-MB231, and Caki-2) were resistant. Knockdown of ADAM28 expression in PC-9 and MDA-MB231 cells by shRNA showed increased carcinoma cell apoptosis mainly in lung blood vessels and statistically significantly decreased lung metastasis at week 3 after injection (PC-9-control [n = 9 mice] vs PC-9-ADAM28-shRNA [n = 9 mice]: mean count = 198×10^6 vs 37×10^6 photons/s, difference = 161×10^6 photons/s, 95% confidence interval = 134×10^6 to 188×10^6 photons/s, $P < .001$). Similar inhibition of lung metastasis was observed with ADAM28-siRNA and anti-ADAM28 antibody.

Conclusion ADAM28 cleaves and inactivates proapoptotic VWF in carcinoma cells and enhances lung metastasis probably by promoting carcinoma cell survival within the blood vessels.

J Natl Cancer Inst 2012;104:906–922

ADAMs (a disintegrin and metalloproteinases) are multifunctional proteins involved in the ectodomain shedding of transmembrane proteins, cell adhesion and migration, and cell signaling (1,2). The human genome contains 25 ADAMs including four pseudogenes, and the 21 ADAM proteins are composed of 13 proteolytic ADAMs that exhibit proteolytic activity and eight nonproteolytic ADAMs (1,3). Proteolytic ADAMs share the metalloproteinase domain of matrix metalloproteinases (MMPs), and a typical proteolytic ADAM protein comprises of propeptide, metalloproteinase, disintegrin-like, cysteine-rich, epidermal growth factor–like, transmembrane, and cytoplasmic domains (3–8). Although the precise biological functions under various pathophysiological conditions remain unclear (3–9), several proteolytic ADAM species, including ADAM8, ADAM9, ADAM12, ADAM15, ADAM17, ADAM19, and ADAM28, are overexpressed in human cancers and are associated with tumor growth and progression (5,9). Our previous studies have indicated that ADAM28 (also known as ADAM metallopeptidase domain 28), which has two alternative isoforms, a prototype membrane–anchored form (ADAM28m) and a short secreted form (ADAM28s) (5,10,11), is abundantly expressed in human non–small cell lung and breast carcinomas (12,13). By in situ hybridization and immunohistochemistry, we have demonstrated that ADAM28 is overexpressed predominantly by carcinoma cells in these carcinoma tissues and that the mRNA expression levels of ADAM28 are associated with the cellular proliferation of breast carcinomas (13) and with both carcinoma cell proliferation and metastasis in the non–small cell lung carcinomas (12). In a parallel study, we showed that serum levels of ADAM28

CONTEXT AND CAVEATS

Prior knowledge

Several ADAMs (a disintegrin and metalloproteinases) expressed in human tumors are associated with tumor growth and cancer progression. ADAM metallopeptidase domain 28 (ADAM28) is overexpressed in human breast and non–small cell lung cancers, but the mechanism of ADAM28-mediated metastasis is not known.

Study design

To search for ADAM28-binding proteins, a yeast two-hybrid system was used to screen the human lung cDNA library, and pro-apoptotic von Willebrand factor (VWF) was identified as a candidate. Effect of ADAM28 on VWF-induced apoptosis was assessed in different human cancer cell lines and also in blood vessels. Effect of inhibition of ADAM28 expression or activity on lung metastasis of human lung cancer and breast cancer cells was investigated using mouse models.

Contribution

ADAM28 cleaved native VWF, and VWF-induced apoptosis was affected by high or low level of ADAM28 expression. Inhibition of ADAM28 expression or activity showed a substantial reduction in lung metastasis and increased apoptosis of cancer cells in the blood vessels.

Implication

ADAM28 inactivates proapoptotic VWF in cancer cells and enhances lung metastasis probably by promoting survival of cancer cells within the blood vessels.

Limitations

ADAM28-induced VWF cleavage and decreased apoptosis may only partly explain its effect on metastasis and other mechanisms could be involved. This study in mice may not be translatable to humans.

From the Editors

in the non–small cell lung carcinoma patients substantially increase with the tumor staging, lymph node metastasis, and carcinoma recurrence (14). These data implicated ADAM28 in cell proliferation and metastasis in the particular human cancers. We have demonstrated that ADAM28 contributes to carcinoma cell proliferation through enhanced bioavailability of insulinlike growth factor I (IGF-I) by selective digestion of IGF-binding protein-3 (IGFBP-3) of the IGF-I/IGFBP-3 complex (13), and to angiogenesis by digestion of connective tissue growth factor in breast carcinomas (15). However, substrates related to metastasis and molecular mechanisms by which ADAM28 promotes metastasis remain elusive.

In this study, we used a yeast two-hybrid system to identify proteins that bind to ADAM28. We examined whether the selected candidate protein was a substrate of ADAM28 and involved in ADAM28-mediated metastasis in experimental models for lung metastasis and spontaneous metastasis.

Materials and Methods

Cell Lines and Cell Culture

Human lung carcinoma (PC-9 and Calu-3), breast carcinoma (MDA-MB231 and MCF-7), renal cell carcinoma (Caki-2 and 769P), and hepatocellular carcinoma (HepG2) cell lines, and non-neoplastic cell lines, which included human mammary epithelial cells (MCF-10A), normal human bronchial epithelial cells (NHBE), human umbilical vascular endothelial cells (HUVEC), Madin–Darby canine kidney cells (MDCK), and BALB/3T3 mouse fibroblasts were used in this study. All cell lines, except PC-9 and NHBE, were purchased from American Type Culture Collection (ATCC) (Manassas, VA), and the ATCC authenticates the phenotypes of these cell lines on a regular basis (http://www.lgcstandards-atcc.org/ATCCScience/AuthenticationandPreservation/tabid/1019/Default.aspx). PC-9 and NHBE cell lines were purchased from Immuno-Biological Laboratories Co, Ltd (Gunma, Japan) and Lonza Walkersville, Inc (Walkersville, MD), respectively. PC-9 cell line is validated for authenticity by European Collection of Cell Culture (https://hpacultures.org.uk/products/celllines/CellLineAuthenticationandQualityControlInformation.jsp). The phenotypes and genotypes of NHBE cell line are authenticated by Lonza Walkersville, Inc, and a certificate is given by Lonza Walkersville, Inc. We did not independently authenticate these cell lines. PC-9, Calu-3, Caki-2, 769P, and HepG2 were cultured in RPMI1640 medium, and MDA-MB231, MCF-7, MDCK, and BALB/3T3 cell lines were cultured in Dulbecco's modified Eagle's medium (DMEM). Both media were supplemented with 10% fetal bovine serum (FBS), 100 U/mL penicillin and 10 μg/mL streptomycin (Sigma-Aldrich, St Louis, MO). MCF-10A cells were cultured in DMEM/F-12 containing 10% FBS and several growth factors (Sigma-Aldrich), and NHBE and HUVEC cells were cultured in their basal media containing 2% FBS according to the instructions of Lonza Walkersville, Inc. 293FT cells for lentiviral transfection were purchased from Invitrogen (Carlsbad, CA) and authenticated by Invitrogen. They were maintained on collagen-coated dishes (Becton, Dickinson and Company, Franklin Lakes, NJ) in DMEM supplemented with 10% FBS.

Yeast Two-Hybrid System: Screening for ADAM28-Binding Proteins

MATCHMAKER Gal4 two-hybrid system 3 and the MATCHMAKER human lung cDNA library were purchased from Clontech Laboratories Inc (Mountain View, CA). cDNA fragment encoding the disintegrin-like (Dis), cysteine-rich (CR), and secreted-specific (SS) domains corresponding to Cys^{410}-Arg^{540} of proADAM28s (the zymogen of ADAM28s) was amplified by polymerase chain reaction (PCR) using human lung cDNA library and the corresponding primers, as described previously by our group (16). The product was cloned into the pGBKT7 vector, generating pGBKT7-Dis/CR/SS (16). The pGBKT7-Dis/CR/SS plasmid was co-introduced into *Saccharomyces cerevisiae* strain AH109 with the human lung cDNA library, and yeast transformants were plated and selected following the manufacturer's (Clontech Laboratories Inc) instructions (16). A total of 215 positive colonies were obtained, plasmids isolated, and *Escherichia coli* strain DH5α was transformed with the plasmids, according to the manufacturer's instructions. The cDNA sequences of all positive clones were determined using a MegaBase 1000 DNA sequencer (Amersham Biosciences Co, Piscataway, NJ). Among the 215 positive clones, 15 were identified as human von Willebrand factor (VWF).

Yeast Two-Hybrid Assay for ADAM28 and VWF Binding

The domain of ADAM28 involved in the interaction with VWF was examined by yeast two-hybrid assays, according to the manufacturer's instructions (Clontech Laboratories Inc). cDNA fragments encoding the Dis, CR, and/or SS domain of ADAM28s were amplified by PCR using pGBKT7-Dis/CR/SS plasmid with the corresponding primers (16). The products were cloned into the pGBKT7 vector, generating pGBKT7-Dis, pGBKT7-CR/SS, and pGBKT7-SS. AH109 was co-transformed with plasmid DNAs encoding different domains of ADAM28s (pGBKT7-Dis/CR/SS, pGBKT7-Dis, pGBKT7-CR/SS, and pGBKT7-SS) and a plasmid encoding the full-length VWF (pACT2-VWF). The transformants were selected and grown as described previously by our group (16,17). Positivity was estimated by visually comparing the growth of yeast transformants with a positive control (transformant carrying pTD1-1 and pVA3-1 plasmids) and a negative control (transformant carrying pGBKT-7 vector alone and pACT2-VWF plasmid).

Binding Assay of proADAM28s to VWF

The purification of VWF from human plasma has been described earlier by our group (18). Microtiter plates with 96-wells (Nalge Nunc International, Rochester, NY) were coated with 100 μL VWF (100, 300, and 500 ng/well) in phosphate-buffered saline (PBS; pH 7.4) prepared from Dulbecco's PBS Tablets (DS Pharma Biomedical, Osaka, Japan) and incubated overnight at 4°C. The plates were washed twice with PBS containing 0.05% Brij 35 and subsequently blocked with 1% bovine serum albumin in PBS for 2 hours at room temperature. Recombinant proADAM28s was purified as described previously (19) and iodinated using iodogen-coated tube (Pierce Biotechnology, Rockford, IL) (19). Briefly, 1–2 μg of recombinant protein was incubated with 200 μCi of $Na^{125}I$ (Amersham Pharmacia Biotech Inc, Piscataway, NJ) and potassium iodide (a final concentration of 0.25 μg/mL) in iodogen-coated tubes for 5 minutes on ice. ^{125}I-labeled proADAM28s (100 ng/well) was incubated in each well for 24 hours at 4°C. After washing twice with PBS containing 0.05% Brij 35, the complex attached to the wells was dissociated by treatment with 1 N NaOH. Radioactivity in the NaOH-dissociated fractions was counted using a gamma counter ARC-600 (Aloka, Tokyo, Japan). Specific binding was determined by competitive inhibition studies using 10- and 50-fold molar excess amount of unlabeled proADAM28s or by incubation with rabbit anti-human VWF polyclonal antibody (5 μg/mL) (Dako, Glostrup, Denmark).

Analysis of VWF Multimeric Pattern

VWF (100 μg/mL) was incubated with or without 1.2 M guanidine hydrochloride overnight at room temperature and then incubated with 10 μg/mL recombinant active ADAM28 (19) or 10 μg/mL ADAMTS13 (a disintegrin and metalloproteinase with a thrombospondin type 1 motif, member 13) (20) for 1 or 18 hours, respectively, at 37°C in reaction buffer (50 mM Tris–HCl buffer [pH 7.5], 10 mM $CaCl_2$, 1 mM phenylmethane sulfonyl fluoride [PMSF], 0.05% Brij 35) or the reaction buffer alone. After termination of the reactions with 10 mM EDTA, a portion of each reaction mixture was analyzed by sodium dodecyl sulfate (SDS)–agarose (1%) gel electrophoresis, and the multimeric state of VWF was visualized by chemiluminescent immunoblotting analysis with rabbit anti-human VWF polyclonal antibody (Dako).

Cleavage of Peptide Substrate by ADAM28 and ADAMTS13

The proteolytic activity of ADAM28 and ADAMTS13 was examined using a fluorescence-quenching substrate, fluorescence resonance energy transfer (FRETS)-VWF73 peptides (Peptide International, Louisville, KY), which contains the 73-amino acids (D^{1596} to R^{1668}) of VWF. Cleavage of this substrate between two modified residues relieves the fluorescence quenching in the intact peptide. ADAM28 (0–50 ng/mL) and ADAMTS13 (0–50 ng/mL) were incubated with 2 μM FRETS-VWF73 in the assay buffer (50 mM Tris–HCl buffer [pH 7.5], 10 mM $CaCl_2$, 150 mM NaCl, 0.05% Brij 35) at 30°C. Proteolysis of the substrate was monitored every 40 seconds up to 30 minutes to obtain the initial rate of fluorescent generation at the excitation 485 nm and the emission 530 nm using the PHERAstar fluorescent microtiter reader (BMG LABTECH, Ortenberg, Germany).

NH_2-Terminal Sequence Analysis of the VWF-Digestion Fragments

VWF was digested with ADAM28 in the reaction buffer (50 mM Tris–HCl buffer [pH 7.5], 10 mM $CaCl_2$, 1 mM PMSF, 0.05% Brij 35) for 18 hours at 37°C, and the digestion products were subjected to gradient (5%–20%) acrylamide gel electrophoresis (ATTO Corporation, Tokyo, Japan). The proteins were transferred onto a polyvinylidene difluoride (PVDF) membrane of 0.2 μm pore size (Millipore, Billerica, MA) and stained with 0.1% Coomassie brilliant blue R-250 (Nakarai Chemicals Ltd, Tokyo, Japan). The bands were excised and sequenced by Edman degradation method using Procise 491 Protein Sequencer (Perkin-Elmer Life Sciences, Waltham, MA).

Reverse Transcription (RT)-PCR

Carcinoma cell lines (PC-9, Calu-3, MDA-MB231, MCF-7, Caki-2, 769P, and HepG2) were grown in their respective medium (described earlier) for 2 days. Total RNA was isolated from the cells using a RNA extraction reagent, Isogen (Nippon Gene Co Ltd, Tokyo, Japan). The RT reaction was performed at 42°C for 60 minutes, followed by heating at 99°C for 5 minutes for inactivation of the enzyme. The cDNAs were amplified by PCR using primers specific for two ADAM28 species (ADAM28s and ADAM28m), ADAMTS13, and housekeeping gene beta-actin (ACTB); primer sequences are shown in Supplementary Table 1 (available online). We used an ExTaq kit from Takara Bio Inc (Shiga, Japan) and a thermal cycler Bio-Rad S1000 Thermal Cycler (Bio-Rad, Hercules, CA); the reaction conditions were initial denaturation at 94°C for 3 minutes, 30 cycles of denaturation for 1 minute at 94°C, annealing for 1 minute at 56°C (ADAM28s and ADAM28m), 58°C (ADAMTS13) or 67°C (ACTB), and extension for 1 minute at 72°C, and a final extension for an additional 3 minutes at 72°C. For detection of distant organ metastasis in a spontaneous metastasis model (see below), RT-PCR for Venus was carried out by the RT reaction using total RNA isolated from mouse organs and the PCR reaction using primers specific for Venus (Supplementary Table 1, available online)

according to the same procedures as mentioned above except for annealing temperature (at 60°C) and PCR cycle (25 cycles). The expected sizes of the amplified cDNA fragments are shown in Supplementary Table 1 (available online). The products were subjected to 2% agarose gel electrophoresis and stained with ethidium bromide.

Immunoblotting

Carcinoma cell lines (PC-9, Calu-3, MDA-MB231, MCF-7, Caki-2, 769P, and HepG2) were grown in their respective media. Cells were homogenized using microhomogenizer Homogenizer Power Plus (LAB, Tokyo, Japan) on ice in 1 mL of lysis buffer (50 mM Tris–HCl buffer [pH 7.5], 10 mM $CaCl_2$, 150 mM NaCl, 0.05% Brij 35 containing a cocktail of proteinase inhibitors) (Roche Diagnostics, GmbH, Mannheim, Germany), and protein concentrations were determined by the dye-binding method using Proteostain Protein Quantification Kit Wide Range (Dojindo Laboratories, Kumamoto, Japan). Homogenate supernatants of carcinoma cells (10 μg total protein per lane) were subjected to SDS-polyacrylamide gel electrophoresis (PAGE) under reducing conditions, and resolved proteins on gels were transferred on to PVDF membranes of 0.2 μm pore size. The membranes were incubated with anti-human ADAM28 mouse monoclonal antibody (297-2F3; 5 μg/mL), which was developed and characterized by our group and is specific to the metalloproteinase domain of ADAM28 (12,13), anti-human ADAMTS13 mouse monoclonal antibody (WH2-11-1; 1 μg/mL), which is specific to the thrombospondin type 1–4 domains of ADAMTS13 (20) or anti-human ACTB mouse monoclonal antibody (0.2 μg/mL) (Sigma-Aldrich) at 4°C for overnight. Antibody binding was detected with the use of horseradish peroxidase (HRP)–conjugated secondary antibodies (1:5000 dilution) (GE Healthcare Bio-Sciences, Uppsala, Sweden). Immunoreactive bands were detected with ECL western blotting reagents (GE Healthcare Bio-Sciences).

To study the effects of a synthetic ADAM inhibitor (KB-R7785; a kind gift from Dr Shintato Inoue, Kanebo, Japan) (19,21) or anti-human ADAM28 mouse monoclonal antibody (297-2F3) on VWF cleavage, carcinoma cell lines were incubated with 3 μg/mL VWF in serum-free DMEM for 48 hours in the presence or absence of 1 μM KB-R7785 or 5 μg/mL anti-ADAM28 antibody. The media (100 μL per lane) were concentrated down to 10 μL by precipitation with ice-cold acetone and then subjected to SDS-PAGE (5%–20% gradient gel) for immunoblotting using rabbit anti-human VWF polyclonal antibody (5 μg/mL) and HRP-conjugated secondary antibody (1:5000 dilution) (GE Healthcare Bio-Sciences).

For analyses of VWF-induced cell signaling, carcinoma cells were incubated with VWF in the presence or absence of 1 μM KB-R7785, anti-human ADAM28 mouse monoclonal antibody (5 μg/mL), anti-human αvβ3 integrin mouse monoclonal antibody (5 μg/mL; Santa Cruz Biotechnology Inc, Santa Cruz, CA), rabbit anti-human αIIb integrin polyclonal antibody (5 μg/mL) (Santa Cruz Biotechnology Inc) or nonimmune IgG (5 μg/mL) (Dako), and supernatants of cell homogenates (10 μg total protein per lane) were subjected to immunoblotting with anti-human phosphorylated tumor protein p53 (p-TP53) mouse monoclonal antibody (0.2 μg/mL) (Cell Signaling Co, Beverly, MA), rabbit anti-human TP53 polyclonal antibody (0.2 μg/mL) (Cell Signaling Co) or rabbit anti-human cleaved caspase-3 (CASP3) polyclonal antibody (0.2 μg/mL) (Millipore). Antibody binding was detected with the use of HRP-conjugated secondary antibodies (1:5000 dilution; GE Healthcare Bio-Sciences).

Apoptosis Assays

DNA Fragmentation Assay. The DNA fragmentation assay was performed by cellular DNA fragmentation enzyme-linked immunosorbent assay (ELISA) (Roche Molecular Biochemicals, Basel, Switzerland). Carcinoma (PC-9, Calu-3, MDA-MB231, MCF-7, Caki-2, 769P, and HepG2) and nonneoplastic (MCF-10A, NHBE, HUVEC, MDCK, and BALB/3T3) cell lines cultured in their respective media were labeled with 5-bromo-2′-deoxy-uridine (BrdU) for 18 hours, and 100 μL of cell suspension (1×10^5 cells/mL) was transferred to each well of a microtiter plate (96 wells, flat bottom). After synchronization and growth arrest, cells were cultured with 3 μg/mL VWF (18) in the presence or absence of 1 μM KB-R7785 for all the cell lines or 5 μg/mL anti-human ADAM28 mouse monoclonal antibody for carcinoma cell lines for 48 hours at 37°C in serum-free medium. For PC-9 cells, the treatment with 3 μg/mL VWF and/or 1 μM KB-R7785 was conducted in RPMI1640 medium containing 10% FBS. The amount of BrdU-labeled DNA released into cell culture supernatants was quantified by ELISA, according to the manufacturer's instructions. To examine whether ADAM28-digested VWF can induce apoptosis, PC-9 cells were treated for 48 hours with ADAM28-digested VWF, which was prepared by incubation of VWF with ADAM28 at a substrate to enzyme ratio of 10:1 at 37°C for 24 hours, and subjected to the DNA fragmentation assay.

DNA Ladder Formation Assay. To assess DNA ladder formation, low–molecular weight DNA was extracted from both detached and adherent cells (2×10^6) or 50 mg of mouse lung tissues using apoptotic DNA ladder isolation kit (Abcam, Cambridge, UK). The extracted DNA fragments were subjected to a 1.2% agarose gel, electrophoresis and analyzed by ethidium bromide staining.

TUNEL Staining. Carcinoma cells were cultured on Lab-Tek chamber slides (Nalge Nunc International) and subjected to terminal deoxynucleotidyl transferase dUTP nick end labeling (TUNEL) staining using apoptag peroxidase in situ apoptosis detection kit (Millipore) according to the manufacturer's recommendation. The number of TUNEL-positive cells was counted in six random high power fields (×40).

Transfection of Cells With ADAM28-Specific Small Interfering RNAs (siRNAs) and Short Hairpin RNAs (shRNAs)

Small Interfering RNA. A 21-oligonucleotide siRNA with the sequence of ADAM28 (5′-AAGACTTCATCCACTGCATAA-3′) and control non-silencing oligonucleotide (5′-AATTCTCGGAA CGTGTCACGT-3′) were custom-synthesized by QIAGEN Inc (Valencia, Santa Clarita, CA) (13). Transfection of PC-9 and MDA-MB231 cells was performed using the Nucleofector Kit (Amaxa Inc, Gaithersburg, MD); siRNA (2 μg) was added to cells (1×10^6) suspended in 100 μL of solution T, which is the transfection

buffer. The cells were then plated in 10-cm plates in RPMI-1640 (for PC-9) and DMEM (for MDA-MB231) media supplemented with 10% FBS, 100 U/mL penicillin, and 10 μg/mL streptomycin. After 48 hours, they were subjected to immunoblotting analysis or apoptosis assays as described above.

Short Hairpin RNA. The shRNA sequence used for knockdown of human ADAM28 was 5′-CACCGCCACAACTTTGGAATG TTTCCGAAGAAACATTCCAAAGTTGTGGC-3′. The lentiviral vectors for ADAM28 shRNA were generated using the BLOCK-iTlentiviral RNAi expression system according to the manufacturer's instructions (Invitrogen). Next, we performed transient transfection of 293FT producer cells (6×10^6) with ADAM28 shRNA–expressing lentiviral vectors (3 μg) using Lipofectamine 2000 (Invitrogen), and supernatants were collected after incubation at 37°C for 2 days. Then the supernatant (50 μL) was filtered using a 0.45 μm Millex filter (Millipore) and added to PC-9 and MDA-MB231 cells (1×10^6), followed by selection and maintenance of transfectants in their respective media containing 10 μg/mL blasticidine (Sigma-Aldrich). Non-targeting shRNA lentiviral vectors (mock) were purchased from Sigma-Aldrich and used as controls.

In Vivo Mouse Metastasis Models for Bioluminescence Imaging, Histology, and Immunohistochemistry

We transfected 293FT cells (6×10^6) with lentiviral expression vectors (3 μg) encoding the fusion protein of firefly luciferase and circularly permutated variant of Venus (a variant of green fluorescent protein [GFP]), named ffLuc-cp156 (22), using Lipofectamine 2000 at 37°C. Two days after transfection, the lentiviral supernatants were collected and filtered using a 0.45 μm Millex filter. For infection, PC-9 and MDA-MB231 cells (1×10^6) were incubated in the virus-containing media (4 μL) for 48 hours, continuously propagated, and then dissociated into single cells. The ffLuc-cp156-positive cells (PC-$9^{ffLuc\text{-}cp156}$ and MDA-$MB231^{ffLuc\text{-}cp156}$ cells) were sorted by a MoFlo cytometer (Dako Cytomation, Carpinteria, CA) and maintained in their respective culture media supplemented with 10% FBS.

Six-week-old male nonobese diabetic/severe combined immunodeficient (NOD/SCID) mice (Charles River Laboratories International Inc, Wilmington, MA) were injected with PC-$9^{ffLuc\text{-}cp156}$ and MDA-$MB231^{ffLuc\text{-}cp156}$ cells (1×10^6 cells in 300 μL PBS) into the tail vein (n = 9 mice per cell line) under anesthesia with isoflurane. Lung metastasis was monitored by bioluminescence imaging using the In Vivo Imaging System (IVIS)-100 camera system for detection of luciferase activity (Xenogen Co, Alameda, CA) according to the manufacturer's instructions. During imaging, mice were anesthetized with isoflurane and received intraperitoneal injection of D-luciferin (150 mg/kg) (Promega Co, Madison, WI), and 1 minute later, photons from the animal whole bodies were counted. Data were analyzed using LIVING IMAGE 3.0 software (Xenogen Co). Housing and maintenance of mice and all procedures were performed according to the guidelines for the Care and Use of Laboratory Animals of School of Medicine (Keio University).

Metastasis in the body was monitored by bioluminescence imaging at 1, 3, 5 days, and 1, 2, 4, 6, and 8 weeks after intravenous injection of PC-$9^{ffLuc\text{-}cp156}$ cells (1×10^6 cells in 300 μL PBS) into the tail vein of mice (n = 3 mice). Mice were killed by cervical dislocation at 8 weeks for full autopsy. After macroscopic observation, whole-visceral organs were dissected out and the organs and trunk were fixed separately in 10% buffered formalin. Tissue specimens were taken from these organs and embedded in paraffin. Paraffin sections (4 μm thick) were stained with hematoxylin and eosin (HE) and also subjected to immunohistochemistry for Venus, which was recognized by rabbit anti-GFP polyclonal antibody (10 μg/mL) (Medical & Biological Laboratories Inc, Nagoya, Japan) for detection of PC-$9^{ffLuc\text{-}cp156}$ cells. Bioluminescence imaging at 8 weeks was compared with macroscopic and microscopic findings obtained by autopsy. Metastasis of MDA-$MB231^{ffLuc\text{-}cp156}$ cells was also examined in a similar way by bioluminescence imaging and full autopsy. For time-course studies of histology and immunohistochemistry of the lungs, the mice (n = 3 mice) were killed at 1, 3, 5 days, and 1, 2, 4, 6, and 8 weeks after intravenous injection of PC-$9^{ffLuc\text{-}cp156}$ cells (1×10^6 cells in 300 μL PBS) into the tail vein of mice, and whole lungs were removed. The formalin-fixed lung tissues were embedded in paraffin, and paraffin sections were subjected to HE staining and immunostaining for Venus as described above. To examine the apoptosis of PC-$9^{ffLuc\text{-}cp156}$ cells within the lung tissues obtained from mice killed at 1 and 3 days after intravenous injection, serial sections (4 μm thick) were made and stained with HE and thiosemicarbazide-periodic acid methenamine silver-hematoxylin (TSC-PAM) (23). They were also subjected to immunohistochemistry for cleaved CASP3 protein using rabbit anti-human cleaved CASP3 polyclonal antibody (20 μg/mL) (Millipore), followed by reactions with EnVision system HRP-labeled polymer anti-rabbit IgG (1:200 dilution) (Dako). Color was developed with 3, 3′-diaminobenzidine tetrahydrochloride (Sigma-Aldrich Co) as described previously (13). After immunohistochemistry, the sections were counterstained with hematoxylin.

Sample size for the above-mentioned experiments was not made on the basis of a power calculation because the primary objective was to compare bioluminescence imaging data with pathological changes and determine the time course of development of lung metastasis. Mice received intravenous injection of PC-$9^{ffLuc\text{-}cp156}$ or MDA-$MB231^{ffLuc\text{-}cp156}$ cells showed marked bioluminescence imaging with multiple organ metastasis at week 8 after the injection. Therefore, the time point at week 8 was chosen as endpoint for monitoring metastasis. We have previously reported that using a xenograft model of MDA-MB231 cells, the control group had a mean tumor volume of 356 mm^3 (SD = 31 mm^3), and the siRNA-treated group had a mean tumor volume of 132 mm^3 (SD = 21 mm^3) (13). Using these numbers as a guide, four mice per group were needed to ensure a power of 80% to detect a difference at alpha level of 0.05. According this calculation, we used 9–10 mice per group for the experiments to analyze effects of ADAM28 knockdown on lung metastasis, primary tumor growth, and spontaneous metastasis (see below).

Effects of ADAM28 Knockdown on Lung Metastasis, Primary Tumor Growth, and Spontaneous Metastasis in Mice

Lung metastasis. For shRNA-mediated approach in a lung experimental metastasis model, we first prepared ADAM28-shRNA

transfectants and mock-transfectants by transfecting PC-9$^{ffLuc\text{-}cp156}$ and MDA-MB231$^{ffLuc\text{-}cp156}$ cells with lentiviral vectors for ADAM28-shRNA or mock (described earlier) and then used these transfectants maintained in their respective medium. NOD/SCID mice were randomly divided into two groups. One group was injected with ADAM28-shRNA transfectants of PC-9$^{ffLuc\text{-}cp156}$ or MDA-MB231$^{ffLuc\text{-}cp156}$ cells (1×10^6 cells in 300 μL PBS) into the tail vein, and the other with mock transfectants (n = 9 mice per group per transfectant). For preparing the siRNA in atelocollagen complex, equal volume of atelocollagen in PBS (Koken Co Ltd, Tokyo, Japan) and siRNA in suspension buffer (QIAGEN Inc) was combined and mixed by rotating for 20 minutes at 4°C. Randomly chosen mice (n = 9 per group) received intravenous injections of 200 μL of 0.05% atelocollagen containing 25 μg of ADAM28 siRNA or non-silencing siRNA at 3, 6, and 9 days after injection of PC-9$^{ffLuc\text{-}cp156}$ cells. To examine the effect of neutralizing anti-ADAM28 antibody on the lung metastasis, PC-9$^{ffLuc\text{-}cp156}$ cells were incubated with 5 μg/mL anti-human ADAM28 mouse monoclonal antibody (297-2F3) (12,13) or 5 μg/mL nonimmune mouse IgG (Dako) for 2 hours at 4°C and then intravenously injected into mice (n = 9 mice per group). From 1 to 3 weeks after the end of the treatment, randomly chosen mice from control and experimental groups were monitored by bioluminescence imaging using the IVIS-100 camera system. To examine the multimeric state of VWF in the arterial blood plasma, blood was collected into tubes containing a 0.1 volume of 3.8% sodium citrate from axillary artery of the mice, which were injected with mock or ADAM28-shRNA transfectants of PC-9$^{ffLuc\text{-}cp156}$ cells. Plasma was prepared by centrifugation at 800*g* for 15 minutes, and VWF multimers were analyzed by chemiluminescent immunoblotting analysis with rabbit anti-human VWF polyclonal antibody after SDS-agarose gel electrophoresis (24). Preparation of plasma from the mice was carried out by a researcher, and immunoblotting analysis was performed by a different investigator, who was blinded to the results of the mouse experiments. As for a positive control, Pooled Normal Plasma (George King Bio-Medical Inc, Overland Park, KS) was used.

Primary Tumor Growth. To assess tumorigenicity, mock and ADAM28-shRNA transfectants of MDA-MB231$^{ffLuc\text{-}cp156}$ and PC-9$^{ffLuc\text{-}cp156}$ cells were implanted in mammary fat pads and subcutaneous tissues of 6- to 8-week-old female NOD/SCID mice (2×10^6 cells per mouse; n = 10 mice per group for MDA-MB231$^{ffLuc\text{-}cp156}$ cells and n = 5 mice per group for PC-9$^{ffLuc\text{-}cp156}$ cells), respectively. Tumor growth in mice randomly chosen from control and experimental groups was monitored every week for 6 weeks by bioluminescence imaging and by measuring tumor volume (13).

Spontaneous Metastasis. Although the mice gave very strong signals in the primary tumors grown in mammary fat pads or subcutaneous tissues at 6 weeks after the injection, evaluation of distant metastasis was difficult by bioluminescence imaging because only weak or negligible signals were detected in other organs corresponding to spontaneous metastasis. Therefore, organ metastases were analyzed by two independent researchers using RT-PCR for the expression of ffLuc-cp156 transcripts using primers specific to Venus (Supplementary Table 1, available online) in the organs including the lung, heart, liver, kidney, and brain isolated from mice at 6 weeks after the cell implantation.

Statistical Analysis

All statistical analyses were performed using a two-tailed Student's *t* test. *P* values less than .05 were considered statistically significant. Data are presented as mean values with 95% confidence intervals (CIs).

Results

Yeast Two-Hybrid and In Vitro Binding Assays to Assess Interaction Between ADAM28 and VWF

The yeast transformants carrying pGBKT7-Dis/CR/SS and pACT2-VWF plasmids or pGBKT7-SS and pACT2-VWF plasmids showed growth similar to the level of positive control (transformant carrying pTD1-1 and pVA3-1 plasmids) on high-stringency plates (Figure 1, A). Weak growth was observed in pGBKT7-CR/SS and pACT2-VWF transformant, whereas growth of pGBKT7-Dis and pACT2-VWF transformant was similar to the negative control (transformant carrying pGBKT7 vector alone and pACT2-VWF plasmid), which showed no growth. Because these results suggested that the CR and/or SS domains of ADAM28 interact with VWF, we performed an in vitro binding assay using ^{125}I-labeled recombinant proADAM28 and purified human VWF and found that binding increased with increase in VWF concentration from 100 to 300 ng, but plateaued after that (Figure 1, B, left panel). The binding was competitively inhibited by addition of unlabeled excess amount of proADAM28 (mean count in control [no excess unlabeled proADAM28] vs 10-fold excess of unlabeled proADAM28: 5270 vs 2875 cpm, difference = 2395 cpm, 95% CI = 1802 to 2988 cpm, $P = .009$; control vs 50-fold excess of proADAM28: 5270 vs 917 cpm, difference = 4353 cpm, 95% CI = 3894 to 4812 cpm, $P = .002$), and suppressed by incubation with anti-VWF antibody as compared with nonimmune IgG (nonimmune IgG vs anti-VWF antibody: 4997 vs 1224 cpm, difference = 3773 cpm, 95% CI = 3537 to 4009 cpm, $P = .002$) (Figure 1, B, right panel).

Cleavage of VWF by ADAM28

When VWF pretreated with guanidine hydrochloride, a denaturant, was incubated with recombinant active ADAM28, ADAMTS13 or buffer alone, both ADAM28 and ADAMTS13 processed VWF into smaller multimers (Figure 2, A, left panel). Under the conditions untreated with guanidine hydrochloride, however, the proteolysis was observed only with ADAM28 (Figure 2, A, right panel). These data demonstrated that ADAM28 could cleave both native and denatured VWF, whereas ADAMTS13 cleaved only denatured VWF, as reported previously (25,26). Confirming the data, a VWF-mimic synthetic peptide was digested with ADAMTS13 in a dose- and time-dependent manner, but resistant to ADAM28 (Figure 2, B). SDS-PAGE analysis showed that ADAM28 digested VWF monomer of approximately 250 kDa into two smaller fragments of 200 and 180 kDa, and NH_2-terminal sequence analysis of these fragments showed that the sequences were L^{1243}VVPPTDA and L^{1483}GVSTLGP, respectively (Figure 2, C). The data indicate that ADAM28 cleaves the Gly^{1242}-Leu^{1243}

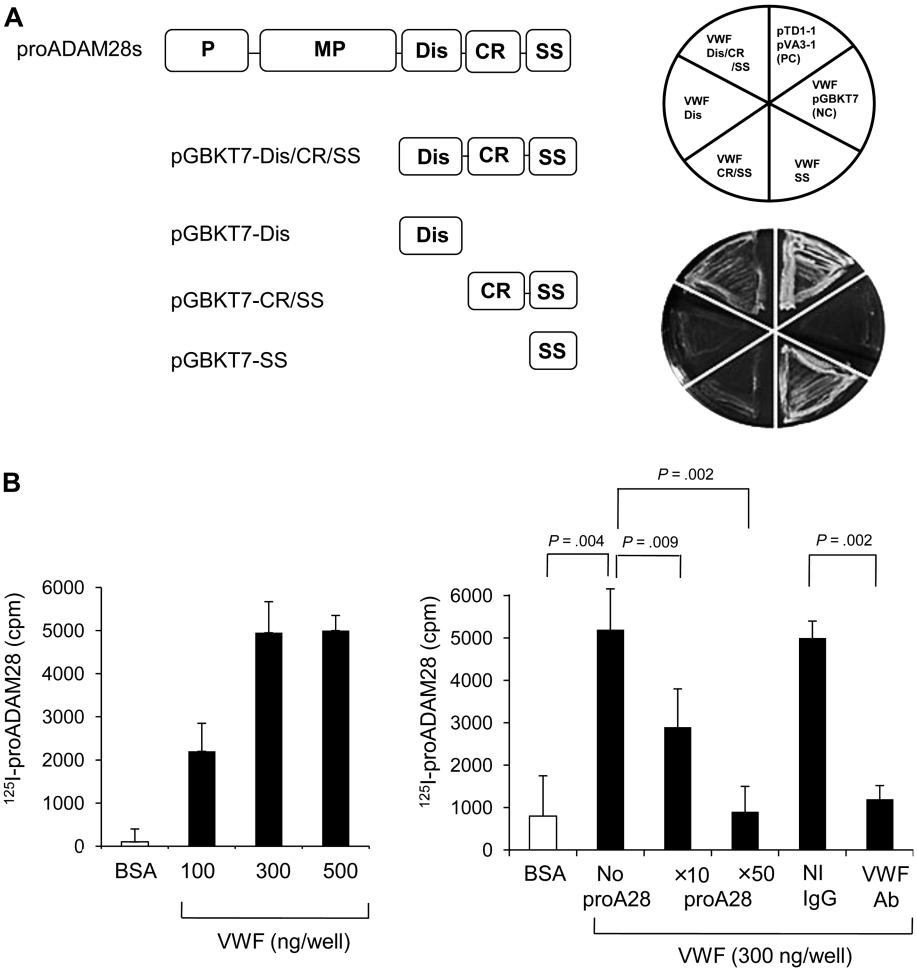

Figure 1. Interaction of ADAM28 with VWF using the yeast two-hybrid assay and in vitro binding assay. **A**) Interaction of ADAM28 fragments with VWF in yeast. Yeast strains were co-transformed with pGBKT7 vector containing ADAM28s fragments (Dis/CR/SS, Dis, CR/SS or SS; bait plasmid) and pACT2-VWF (VWF; hunter plasmid), and cultured for 2 days on yeast minimal medium lacking leucine, tryptophan, histidine, and adenine. The transformants containing both bait and hunter plasmids could grow and survive in the yeast minimal media. Positivity was estimated visually comparing the growth of transformants with pTD1-1 and pVA3–1 plasmids, used as positive control (PC), and transformants with pGBKT7 vector alone and pACT2-VWF plasmid, used as negative control (NC). **B**) Binding assay for ADAM28 and VWF. ^{125}I-proADAM28s was incubated in bovine serum albumin (BSA) or VWF-coated wells (100, 300, or 500 ng/mL), and relative binding ratios were calculated by counting radioactivity (left panel). Inhibition studies were carried out in VWF-coated wells (300 ng/mL) by using 10- and 50-fold molar excess (×10 proA28 and ×50 proA28) amount of unlabeled proADAM28s (proA28) or 5 μg/mL anti-VWF antibody (Ab) (right panel). The means and **error bars** representing 95% confidence intervals from three independent experiments in triplicate are presented. *P* values were calculated using two-sided Student's *t* test. ADAM28 = a disintegrin and metalloproteinase 28; CR = cysteine-rich domain; Dis = disintegrin-like domain; MP = metalloproteinase domain; NI = nonimmune; P = propeptide domain; SS = secreted-specific domain; VWF = von Willebrand factor.

bond in the linker region between D3 and A1 domains and the Leu[1482]-Leu[1483] bond between A1 and A2 domains of VWF protein (27) (Figure 2, D).

Analysis of Apoptosis in VWF-Treated Human Carcinoma Cell Lines

VWF is reported to induce apoptosis of mouse cancer cell lines such as B16BL6 melanoma and Lewis lung carcinoma cells (28). Therefore, we first examined VWF-induced apoptosis by DNA fragmentation assay in seven human carcinoma cell lines (PC-9, Calu-3, MDA-MB231, MCF-7, Caki-2, 769P, and HepG2) and five non-neoplastic cell lines (MCF-10A, NHBE, HUVEC, MDCK, and BALB/3T3). Among the carcinoma cell lines, only MCF-7, 769P, and HepG2 showed VWF-induced apoptosis; no induction of apoptosis was observed in the non-neoplastic cell lines (data not shown). Carcinoma cell lines, except for MCF-7, 769P, and HepG2, demonstrated mRNA and protein expression of ADAM28 (Figure 3, A; data not shown for Calu-3 and 769P cells), whereas none of the cell lines except for HepG2 cells expressed ADAMTS13 (Figure 3, A). When carcinoma cell lines with no or very low-level expression of ADAM28 (MCF-7, 769P, and HepG2 cells) were cultured in presence of 3 μg/mL VWF under serum-free condition and labeled with BrdU, we observed a statistically significant increase in DNA fragmentation (mean relative absorbance levels in control vs VWF-treated cells: MCF-7, 0.46 vs 1.32, difference = 0.86, 95% CI = 0.73 to 0.99, *P* = .007; HepG2, 0.22 vs 0.79, difference = 0.57, 95% CI = 0.42 to 0.72, *P* = .006) (Figure 3, B; data not shown for 769P cells). On the other hand, cell lines expressing ADAM28 (PC-9, Calu-3, MDA-MB231, and Caki-2 cells) were resistant to VWF-induced DNA fragmentation under the same conditions (Figure 3, B; data not shown for Calu-3). However, these resistant cell lines exhibited statistically significantly increased DNA fragmentation when they were treated with VWF in presence of KB-R7785, an ADAM inhibitor (mean relative absorbance levels in control vs VWF + KB-R7785: PC-9, 0.40 vs 1.27, difference = 0.87, 95% CI = 0.68 to 1.06, *P* = .005; MDA-MB231, 0.32 vs 0.82, difference = 0.50, 95% CI = 0.36 to 0.64, *P* = .009; Caki-2, 0.39 vs 0.95, difference = 0.56, 95% CI = 0.44 to 0.68, *P* = .004) (Figure 3, B; data not shown for Calu-3 and 769P cells). The number of TUNEL-positive cells per total cells increased after treatment with VWF and KB-R7785 compared with VWF alone (mean percentage of TUNEL-positive cells for VWF vs VWF + KB-R7785: PC-9, 3.2% vs 21.2%, difference = 18%, 95% CI = 14.7% to 21.3%, *P* < .001; Calu-3, 4.2% vs 14.3%, difference = 10.1%, 95% CI = 7.3% to 12.9%, *P* < .001; MDA-MB231, 5.6% vs 24.5%, difference = 18.9%, 95% CI = 16.5% to 21.3%, *P* < .001; and Caki-2, 5.2% vs 16.2%, difference = 11%, 95% CI = 8.6% to 13.4%, *P* < .001) (Figure 3, C, for PC-9 cells; data not shown for other cell lines). VWF-induced apoptosis was also supported by DNA ladder formation in PC-9

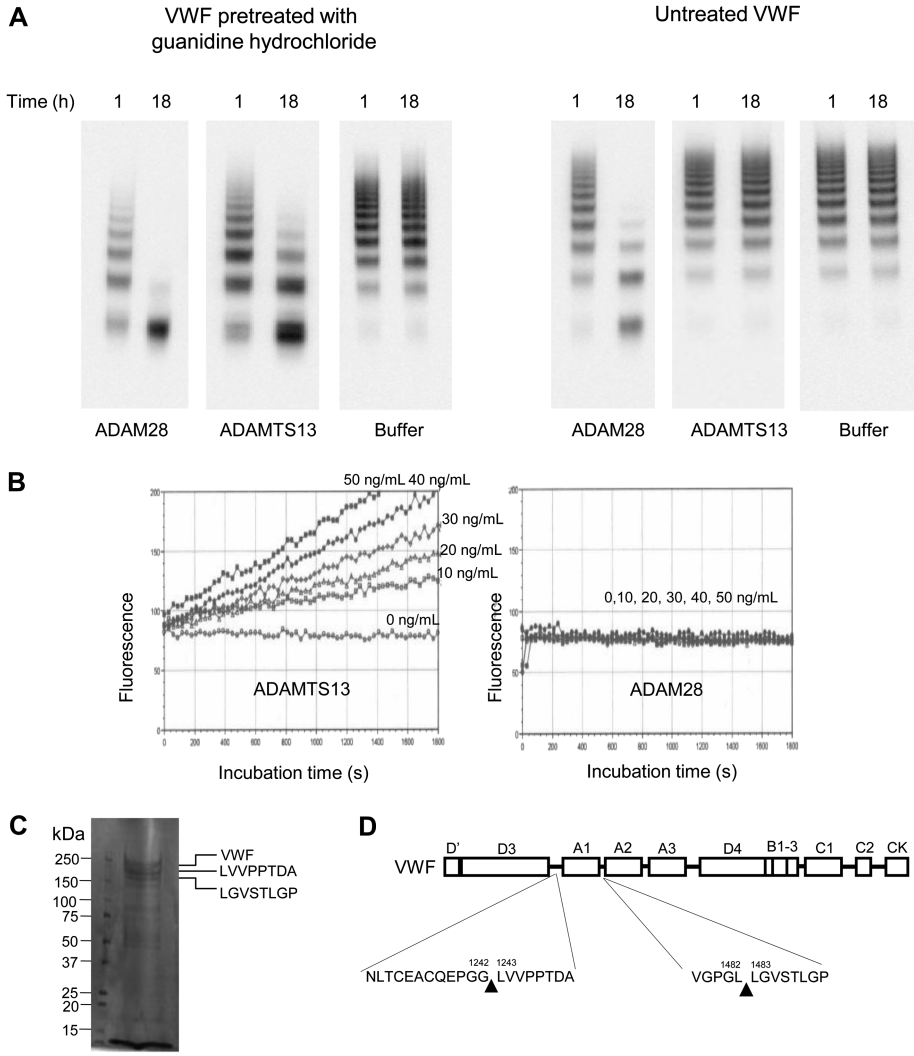

Figure 2. Comparison of digestion patterns of VWF and a synthetic peptide substrate by ADAM28 and ADAMTS13, and analysis of VWF cleavage sites. **A**) Analysis of VWF multimers after digestion with ADAM28 or ADAMTS13. VWF pretreated with or without guanidine hydrochloride was incubated for 1 or 18 hours (h) with recombinant active ADAM28, ADAMTS13 or buffer alone, and the digestion was determined by analysis of VWF multimers by immunoblotting with rabbit anti-human VWF polyclonal antibody. Each image is derived from the same gel. Representative result from three independent experiments is shown. **B**) Activity of ADAMTS13 and ADAM28 toward a synthetic substrate for ADAMTS13 (FRETS-VWF73 peptides). FRETS-VWF73 peptide was incubated with increasing concentrations (0–50 ng/mL) of ADAMTS13 or ADAM28, and proteolysis of the substrate was monitored by a fluorescent microtiter reader. Representative result from three independent experiments is shown. **C**) NH_2-terminal sequence analysis of the cleavage sites of VWF by ADAM28. VWF digested with ADAM28 was analyzed by sodium dodecyl sulfate–polyacrylamide gel electrophoresis. The protein bands of VWF and digestion fragments stained with Coomassie brilliant blue were subjected to NH_2-terminal sequence analysis by Edman degradation method. The experiment was performed only once. The NH_2-terminal sequences of the 200- and 180-kDa fragments are shown on the right. **D**) A schematic diagram shows the domain structure of VWF and VWF cleavage sites by ADAM28 in the linker regions between D3 and A1 domains and A1 and A2 domains. ADAM28 = a disintegrin and metalloproteinase 28; ADAMTS13 = a disintegrin and metalloproteinase with a thrombospondin type 1 motif, member 13; VWF = von Willebrand factor.

cells that were treated with VWF and KB-R7785 (Figure 3, D). Although the experiments for VWF-induced apoptosis were carried out under serum-free conditions, enhanced apoptosis was also observed by treatment of PC-9 cells with 3 μg/mL VWF and KB-R7785 in RPMI-1640 containing 10% FBS (data not shown).

Because these data demonstrated that VWF-induced apoptosis occurs only when ADAM28 expression is absent or the metalloproteinase activity is blocked, we further examined whether ADAM28 was directly involved in escaping VWF-induced apoptosis by degrading this proapoptotic factor. When ADAM28-expressing PC-9 and MDA-MB231 cells were treated with VWF in presence of ADAM inhibitor KB-R7785 or neutralizing anti-ADAM28 antibody, a statistically significantly increased apoptosis was observed compared with the control cells (mean relative absorbance levels in PC-9 cells: no inhibitor vs KB-R7785-treated cells, 0.5 vs 1.5, difference = 1.0, 95% CI = 0.8 to 1.2, P = .004; nonimmune IgG vs anti-ADAM28 antibody-treated cells, 0.3 vs 1.6, difference = 1.3, 95% CI = 1.1 to 1.5, P =.001) (Figure 3, E; Supplementary Figure 1, available online, for MDA-MB231 cells). Knockdown of ADAM28 expression by siRNA in PC-9 and MDA-MB231 cells (Supplementary Figure 2, available online) showed statistically significantly increased VWF-induced apoptosis compared with the non-silencing siRNA (mean relative absorbance levels in non-silencing siRNA vs ADAM28 siRNA in PC-9: 0.53 vs 1.4, difference = 0.87, 95% CI = 0.73 to 1.01, P = .003) (Figure 3, E and Supplementary Figure 1, available online). Consistent with the data, immunoblot analysis showed that VWF degradation was reduced in PC-9 cells when ADAM28 expression was blocked using specific siRNA (Figure 3, F). On the other hand, VWF digestion was negligible in HepG2 cells (Figure 3, G), which were sensitive to VWF-induced apoptosis and expressed ADAMTS13, but not ADAM28 (Figure 3, A and B). In addition, PC-9 cells showed negligible apoptosis, when they were treated with ADAM28-digested VWF in the presence or absence of KB-R7785 (data not shown). These data strongly suggest that the ADAM28-dependent degradation of native VWF in carcinoma cells plays a crucial role in escaping VWF-induced apoptosis. At the same time, we have shown that ADAMTS13 secreted from HepG2 cells was unable to prevent the VWF-induced apoptosis because it could not cleave native VWF.

Mechanism of VWF-Induced Apoptosis

Because VWF can bind to tumor cells via integrins αvβ3 (29,30) and/or αIIbβ3 (31), we examined the expression of these integrins

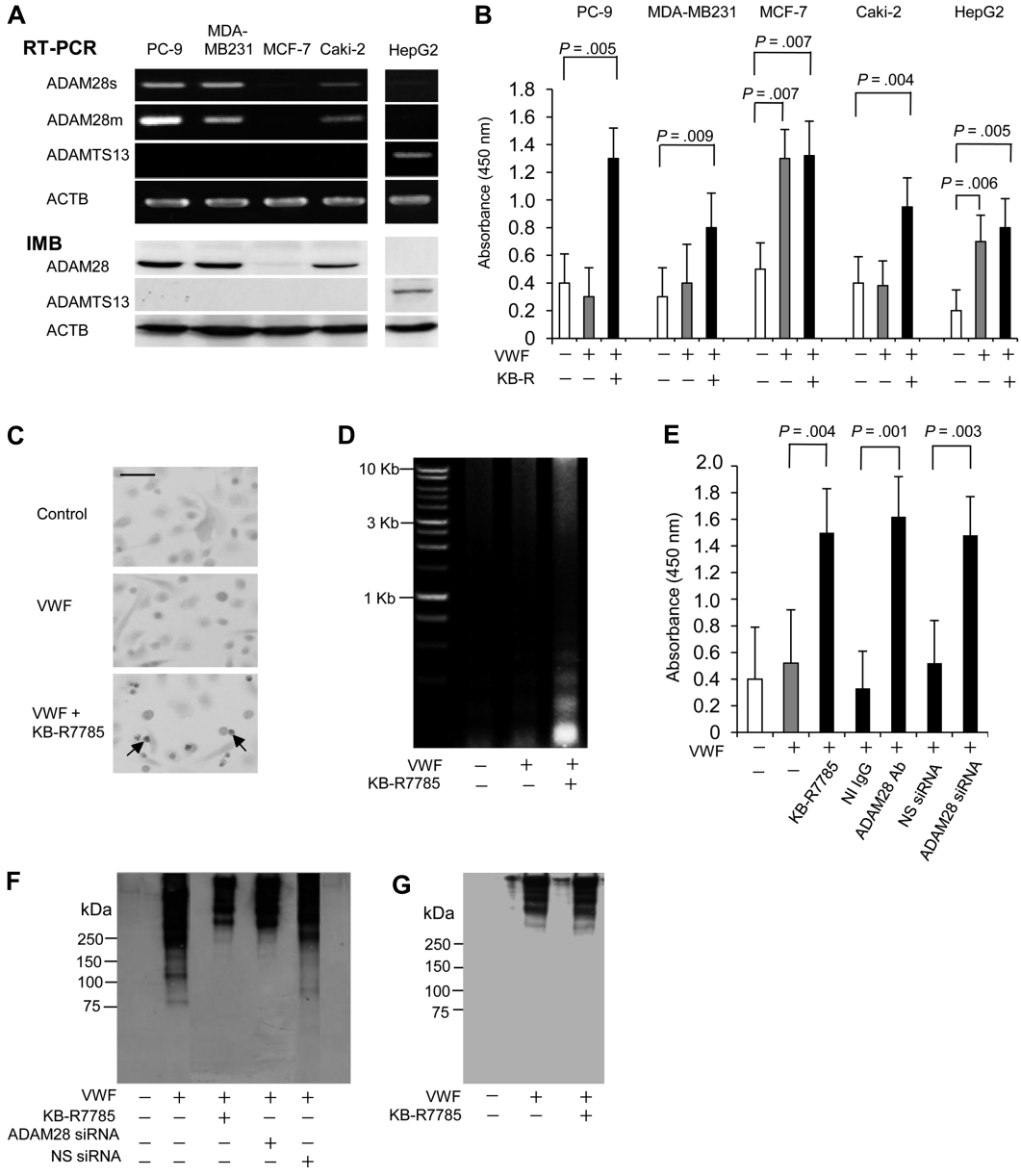

Figure 3. Effect of VWF cleavage by ADAM28 on VWF-induced apoptosis in human carcinoma cell lines. **A**) Expression of ADAM28 and ADAMTS13 in human carcinoma cell lines. The expression was examined by RT-PCR and IMB. ACTB was used as the loading control. Data from five representative cell lines are shown. Representative results from three independent experiments are presented. **B**) VWF-induced apoptosis in human carcinoma cell lines with high-level expression (PC-9, MDA-MB231, and Caki-2) or very low-level expression of ADAM28 (MCF-7 and HepG2). The cells were incubated with 3 μg/mL VWF alone or 3 μg/mL VWF plus 1 μM KB-R7785 (KB-R; an ADAM inhibitor) and then analyzed for apoptosis by DNA fragmentation enzyme-linked immunosorbent assay (ELISA). The means and **error bars** representing 95% confidence intervals derived from five different experiments in triplicate are presented. *P* values were calculated using two-sided Student's *t* test. **C**) Terminal deoxynucleotidyl transferase dUTP nick end labeling (TUNEL) staining of PC-9 cells after treatment with buffer alone (control), 3 μg/mL VWF or 3 μg/mL VWF plus 1 μM KB-R7785. The representative images of each group are shown. **Arrows** indicate TUNEL-positive cells. The cultures were performed in triplicate and the experiments were repeated two times. **D**) DNA ladder formation in PC-9 cells after treatment with VWF plus KB-R7785. The cells were incubated with 3 μg/mL VWF alone or 3 μg/mL VWF plus 1 μM KB-R7785 and then analyzed for apoptosis by DNA ladder formation on an agarose gel stained with ethidium bromide. Representative result from three independent experiments is shown. **E**) VWF-induced apoptosis in PC-9 cells after inhibition of ADAM28 activity or expression. PC-9 cells were incubated with 3 μg/mL VWF in the presence of 5 μg/mL anti-human ADAM28 mouse monoclonal antibody or 5 μg/mL nonimmune (NI) IgG and analyzed for apoptosis by DNA fragmentation ELISA. Similarly, they were transfected with ADAM28-specific small interfering RNA (siRNA) or non-silencing (NS) siRNA, incubated with 3 μg/mL VWF and then subjected to DNA fragmentation ELISA. The means and **error bars** representing 95% confidence intervals from five independent experiments in triplicate are presented. *P* values were calculated using two-sided Student's *t* test. **F**) VWF digestion by treatment with KB-R7785 or siRNA for ADAM28 in PC-9 cells. VWF (3 μg/mL) was added to culture media of PC-9 cells that had been treated with buffer alone, 1 μM KB-R7785, siRNA for ADAM28 or NS siRNA. Conditioned media were immunoblotted for VWF with rabbit anti-human VWF polyclonal antibody. Representative result from two independent experiments is shown. **G**) Digestion of VWF in HepG2 cells. VWF (3 μg/mL) was added to culture media of HepG2 cells in the absence or presence of 1 μM KB-R7785, and conditioned media were immunoblotted for VWF. The experiments were repeated two times and representative result is shown. ACTB = beta-actin; ADAM28 = a disintegrin and metalloproteinase 28; ADAM28m = membrane-anchored form of ADAM28; ADAM28s = a short secreted form of ADAM28; ADAMTS13 = a disintegrin and metalloproteinase with a thrombospondin type 1 motif, member 13; IMB = immunoblot; VWF = von Willebrand factor; RT-PCR = reverse transcription-polymerase chain reaction.

and found that PC-9 and MDA-MB231 cells express αvβ3 integrin but not αIIbβ3 integrin (Supplementary Figure 3, available online). Binding of resveratrol (a polyphenol) and canstatin (noncollagenous domain of type IV collagen α-chains) to αvβ3 integrin is known to induce apoptosis in human breast carcinoma cell lines through phosphorylation of TP53 (32) and activation of CASP3 (33), respectively. Therefore, we explored these cell signaling pathways and found that treatment of PC-9 cells with VWF and KB-R7785 induced TP53 phosphorylation and CASP3 activation (indicated by cleavage) together with apoptosis (measured by DNA fragmentation assay), although VWF alone showed neither activation of such molecules nor apoptosis (Figure 4, A and B). Importantly, the induction of apoptosis was statistically significantly inhibited (P = .010) when PC-9 cells were treated with anti-αvβ3 integrin antibody before treating them with VWF and KB-R7785 (Figure 4, B). Under these conditions, the antibodies or KB-R7785 alone had no effect on cell signaling or apoptosis. Similar results were obtained using MDA-MB231 cells (Supplementary Figure 4, B, available online). All these data indicate that VWF binding to αvβ3 integrin induces apoptosis in PC-9 and MDA-MB231 cell lines by stimulation of the downstream signaling pathway involving phosphorylation of TP53 and activation of CASP3.

Analysis of Lung Metastasis in a Mouse Model

More than 90% of PC-9$^{ffLuc\text{-}cp156}$ cells (overall median = 91%, range = 85%–97%) (Figure 5, A) and MDA-MB231$^{ffLuc\text{-}cp156}$ cells (overall median = 92%, range = 87%–97%) (Supplementary Figure 5, A, available online) showed stable positive staining for Venus, analyzed by fluorescence microscopy. When NOD/SCID mice (n = 3) injected intravenously with PC-9$^{ffLuc\text{-}cp156}$ cells were monitored for lung metastasis by bioluminescence imaging, positive imaging was obtained in the lungs between day 1 and week 1, and additional positive signals besides lungs emerged in the neck and lower abdomen between week 2 and week 8 after the injection (Figure 5, B). Autopsy of the mouse conducted at week 8 demonstrated macroscopically metastatic tumors in the neck and trunk (Figure 5, C, left panel). Microscopically, metastatic tumor cells were detected within the lung and soft tissues (striated muscle) in the neck and trunk by HE staining, and most tumor cells were immunostained for Venus using a rabbit anti-GFP polyclonal antibody (Figure 5, C, right panel). The autopsy data at week 8 confirmed the bioluminescence imaging results. The time course of development of lung metastasis by histological and immunohistochemical analysis of Venus on serial paraffin sections indicated that tumor cells make embolization within the alveolar capillaries on days 1 and 3, extravasate on day 5 and at week 1, and then form the definite metastatic foci within the lung tissues after week 2 and week 4 (Figure 5, D; data not shown for lungs on days 3 and 5). Similar time course of development of metastasis to the lungs, soft tissues, and bone was observed when MDA-MB231$^{ffLuc\text{-}cp156}$ cells were intravenously injected (Supplementary Figure 5, B and C, available online).

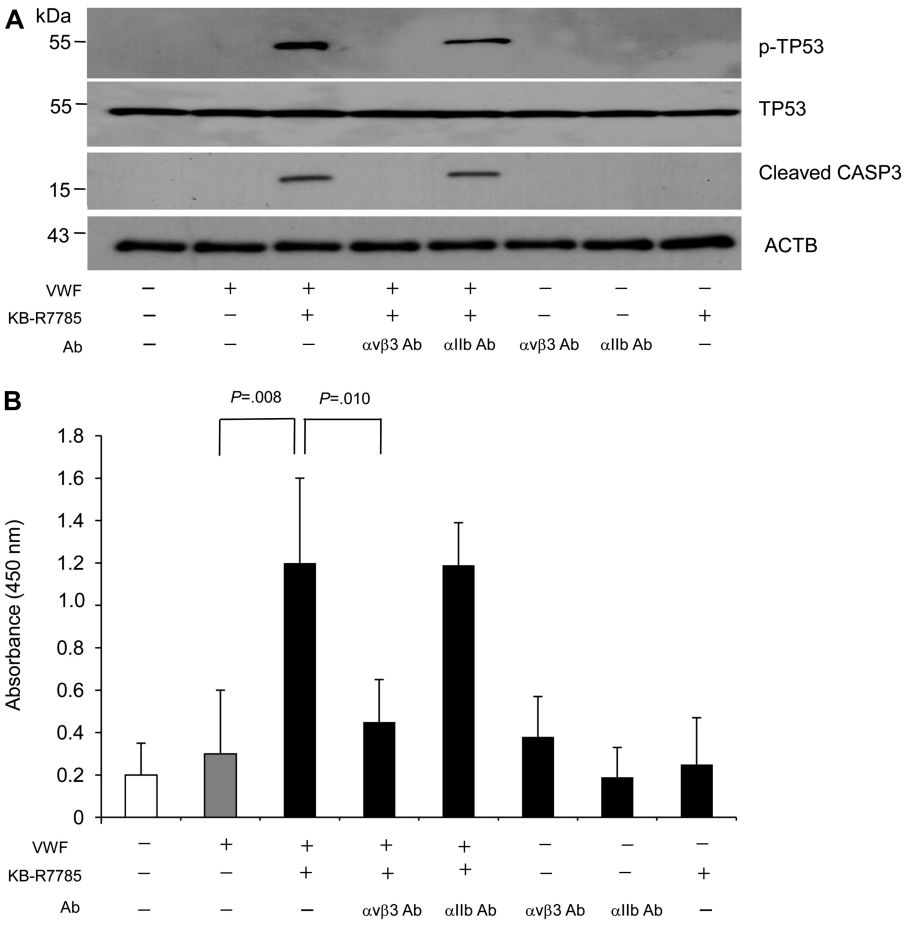

Figure 4. VWF-induced cell signaling pathways for apoptosis via binding to integrin αvβ3. **A**) Activation of TP53 and CASP3 in PC-9 cells treated with VWF plus KB-R7785 and effects of anti-human αvβ3 integrin mouse monoclonal antibody on the activation. PC-9 cells were treated with buffer alone, 3 μg/mL VWF or 3 μg/mL VWF plus 1 μM KB-R7785 (an ADAM inhibitor), and TP53 phosphorylation and activation of CASP3 were determined by immunoblotting with anti-human phophorylated TP53 mouse monoclonal antibody and rabbit anti-human cleaved CASP3 polyclonal antibody, respectively. Phosphorylation of TP53 and activation of CASP3 were also examined in the cells treated with 5 μg/mL anti-human αvβ3 integrin mouse monoclonal antibody or 5 μg/mL rabbit anti-human αIIb integrin polyclonal antibody before treatment with 3 μg/mL VWF plus 1 μM KB-R7785. Anti-αvβ3 antibody, anti-αIIb antibody or KB-R7785 alone is negative controls. ACTB was used as a loading control. **B**) VWF-induced apoptosis by treatment with VWF and KB-R7785 and effect of anti-human αvβ3 integrin antibody on apoptosis. PC-9 cells were treated as described above, and apoptosis was determined by DNA fragmentation enzyme-linked immunosorbent assay. The means and **error bars** representing 95% confidence intervals from three independent experiments are presented. *P* values were calculated using two-sided Student's *t* test. Ab = antibody; ACTB = beta-actin; CASP3 = caspase 3; TP53 = tumor protein p53; VWF = von Willebrand factor.

Effect of Knockdown of ADAM28 Expression or Activity on Lung Metastasis

Next, we assessed knockdown of ADAM28 expression after transfection of PC-9$^{ffLuc\text{-}cp156}$ cells with ADAM28-shRNA (shADAM28) or mock-shRNA lentiviral vectors. Both RT-PCR and immunoblot analysis showed that ADAM28 expression was effectively suppressed in ADAM28-shRNA transfectants compared with mock-shRNA transfectants (Figure 6, A and Supplementary Figure 5, D, available online). When shADAM28 or mock transfectants of PC-9$^{ffLuc\text{-}cp156}$ cells were intravenously injected in mice, a statistically significantly reduced lung metastasis was observed with ADAM28-specific shRNA compared with mock shRNA at week 2 and week 3 after injection (mean photon counts in mock [n = 9 mice] vs shADAM28 [n = 9 mice] at week 3: 198 × 10^6 vs 37 × 10^6 photons/s, difference = 161 × 10^6 photons/s, 95% CI = 134 × 10^6 to 188 × 10^6 photons/s, $P < .001$) (Figure 6, B). The ADAM28-shRNA transfectants of MDA-MB231$^{ffLuc\text{-}cp156}$ cells showed similar inhibitory effects on metastasis (Supplementary Figure 5, E, available online). When lung tissues from mice (n = 6 per group) were analyzed for apoptosis, enhanced apoptosis of the ADAM28-shRNA transfectants, but not mock transfectants of PC-9$^{ffLuc\text{-}cp156}$ cells, was indicated by appearance of typical DNA ladder (Figure 6, C). In addition, the expression level of cleaved CASP3 increased in the lung tissues from mice in the shADAM28 group compared with the mock group (Figure 6, D). A densitometric analysis of the immunoreactive band of cleaved CASP3 demonstrated statistically significantly increased expression in the ADAM28-shRNA group compared with the mock group (n = 9 mice per group) (shADAM28 vs mock: 5.2- vs 1.0-fold change, difference = 4.2-fold change, 95% CI = 2.9- to 5.5-fold change, $P < .001$). Lung sections were stained with HE and TSC-PAM to analyze localization of PC-9$^{ffLuc\text{-}cp156}$ cells within the blood vessels. Sections stained with TSC-PAM demonstrated that a large percentage of PC-9$^{ffLuc\text{-}cp156}$ cells were located within the blood vessels on day 1 (overall median = 95%, range = 91%–98%; n = 6 mice) and day 3 (overall median = 90%, range = 83%–94%; n = 6 mice) after intravenous injection (Figure 6, E). Immunohistochemistry analysis of lung sections for cleaved CASP3 showed positive staining in mice injected with ADAM28-shRNA–transfected PC-9$^{ffLuc\text{-}cp156}$ cells and located mainly within the blood vessels of the lungs on day 3, whereas only weak staining was observed in mice injected with mock transfectants (n = 3 mice per group) (Figure 6, F). Negligible immunostaining was observed in

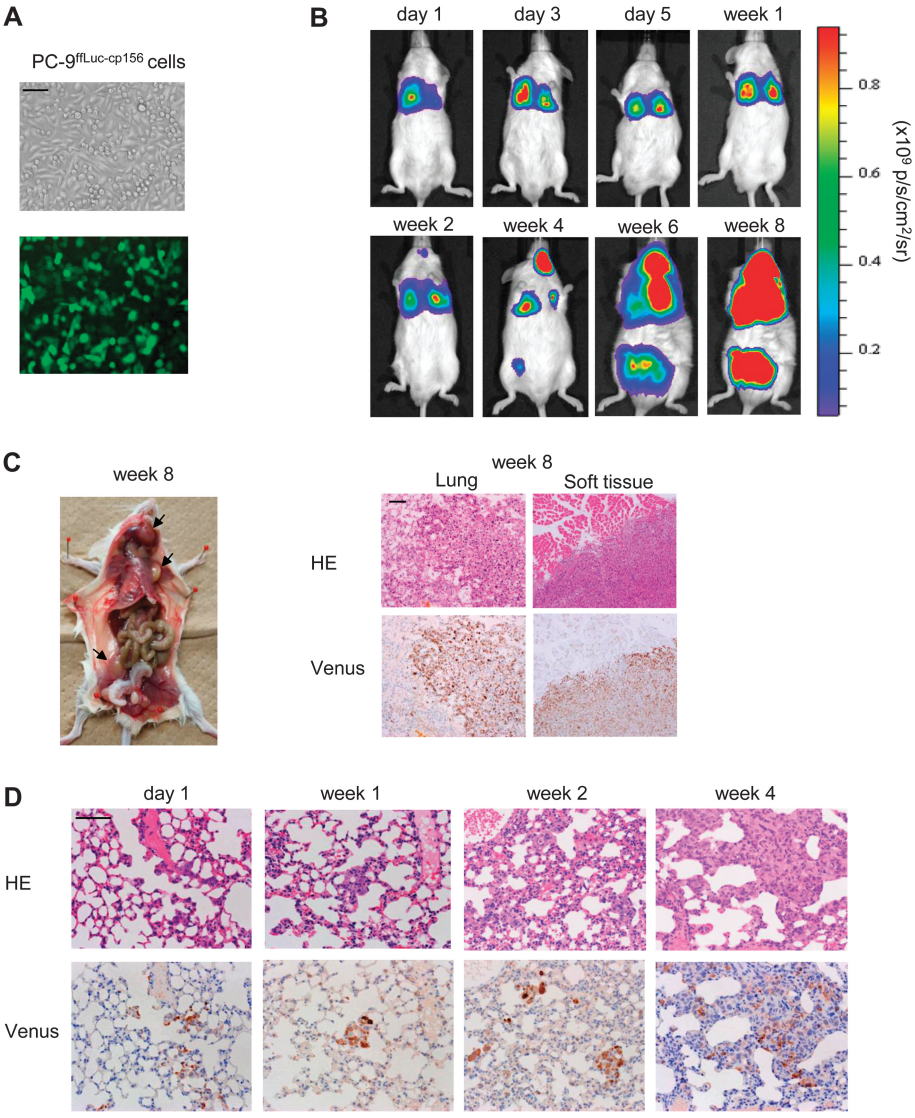

Figure 5. Development of a lung metastasis model in mice using PC-9$^{ffLuc\text{-}cp156}$ cells. **A**) Generation of PC-9$^{ffLuc\text{-}cp156}$ cells. PC-9 cells were stably transfected with the lentiviral vectors encoding the fusion protein of firefly luciferase and circularly permutated variant of Venus (a variant of green fluorescent protein [GFP]), named ffLuc-cp156. Representative images by phase contrast microscopy (upper panel) and fluorescence microscopy for Venus (lower panel) are shown. Scale bar = 100 μm. **B**) Time-course changes of bioluminescence imaging of the metastasis in a male nonobese diabetic/severe combined immunodeficient mouse. PC-9$^{ffLuc\text{-}cp156}$ cells were injected to tail vein of a mouse, and metastases were monitored by bioluminescence imaging using IVIS-100 camera system. Representative imaging data on a mouse from three independent experiments are shown. **C**) Macroscopic and microscopic findings of the same mouse shown in (**B**). The mouse was autopsied at week 8 after the intravenous injection of PC-9$^{ffLuc\text{-}cp156}$ cells. Left panel shows the macroscopic finding of metastatic tumors in the soft tissues (**arrows**). Right panel indicates metastatic tumors in the lung and soft tissue (striated muscle), which were stained with hematoxylin and eosin (HE) and immunostained for Venus with rabbit anti-GFP polyclonal antibody. Representative result from three independent experiments is shown. Scale bar = 100 μm. **D**) Time-course of development of lung metastasis. The lung tissues were obtained from mice at day 1 and weeks 1, 2, and 4 after intravenous injection of PC-9$^{ffLuc\text{-}cp156}$ cells and evaluated by HE staining and immunohistochemistry for Venus with rabbit anti-GFP polyclonal antibody on serial paraffin sections. Scale bar = 100 m.

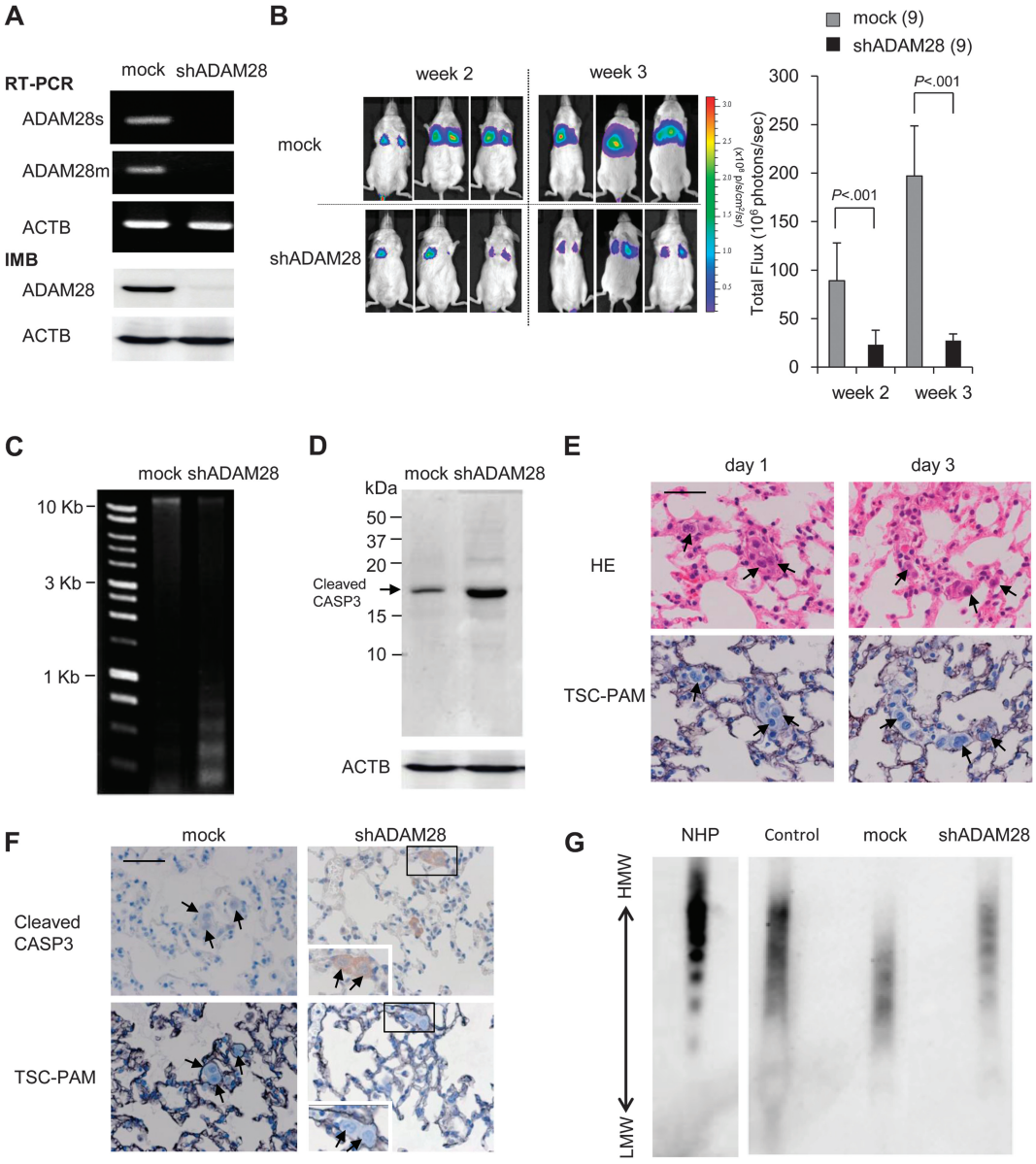

Figure 6. Knockdown of ADAM28 expression using short hairpin RNA (shRNA) and effect on lung metastasis. **A**) Expression of ADAM28 in PC-9$^{ffLuc\text{-}cp156}$ cells transfected with lentiviral vectors of shRNA for ADAM28 (shADAM28) or mock vectors (mock). The expression of ADAM28 mRNA and protein was determined by RT-PCR and IMB, respectively. ACTB was used as a loading control. **B**) Lung metastasis study. Nonobese diabetic/severe combined immunodeficient (NOD/SCID) mice (n = 3 per group) were injected intravenously with mock- and shADAM28-transfectants (shADAM28) of PC-9$^{ffLuc\text{-}cp156}$ cells, and lung metastasis was determined by bioluminescence imaging at week 2 and week 3 after injection. Mean values and upper 95% confidence intervals from three independent experiments are shown in the **bar graph**. The total number of mice in each group is shown in **parentheses**. **C**) DNA ladder formation in the mouse lung tissues. Lung tissues were obtained from NOD/SCID mice (n = 3 per group) on day 3 after injection with mock- and shADAM28-transfectants of PC-9$^{ffLuc\text{-}cp156}$ cells. Low–molecular weight DNA was extracted from the tissues, and DNA ladder formation was detected by staining the agarose gel with ethidium bromide. Results were generated from three independent experiments, and representative result is presented. **D**) Immunoblot analysis of cleaved CASP3 in the mouse lung tissues. The lung tissues were removed from NOD/SCID mice on day 3 after intravenous injection of mock- and shADAM28-transfectants of PC-9$^{ffLuc\text{-}cp156}$ cells, and homogenate supernatants were subjected to immunoblotting with rabbit anti-human cleaved CASP3 polyclonal antibody. Experiments were performed for lung samples from nine mice per group. ACTB was used as the loading control. **E**) Histological analysis of the lung tissue. The lung samples were obtained from mice (n = 3) on day 1 and day 3 after intravenous injection of mock-transfectants of PC-9$^{ffLuc\text{-}cp156}$ cells. Serial paraffin sections were stained with HE and TSC-PAM. Scale bar = 100 μm. **Arrows** indicate PC-9$^{ffLuc\text{-}cp156}$ cells within blood vessels. **F**) Immunohistochemistry of cleaved CASP3 in the lung tissues on day 3 after injection of mock- and shADAM28-transfectants (shADAM28) of PC-9$^{ffLuc\text{-}cp156}$ cells. Serial sections were stained with rabbit anti-human cleaved CASP3 polyclonal antibody and TSC-PAM. **Arrows** indicate PC-9$^{ffLuc\text{-}cp156}$ cells within blood vessels. Scale bar = 100 μm. Higher magnification of boxed areas outlined in black are shown in insets. **G**) Analysis of VWF multimers in mice plasma samples. Plasma was obtained from mice on day 2 after the injection with PBS alone (control), mock-transfectants (mock), or shADAM28-transfectants (shADAM28) (n = 3 mice per group). The plasma samples were subjected to chemiluminescent immunoblotting analysis using rabbit anti-human VWF polyclonal antibody. ACTB = beta-actin; ADAM28 = a disintegrin and metalloproteinase 28; ADAM28m = membrane-anchored form of ADAM28; ADAM28s = a short secreted form of ADAM28; HE = hematoxylin and eosin; IMB = immunoblot; HMW = high molecular weight; LMW = low molecular weight; NHP = normal human plasma (positive control for large VWF multimers); RT-PCR, reverse transcription-polymerase chain reaction; TSC-PAM = thiosemicarbazide-periodic acid methenamine silver-hematoxylin; VWF = von Willebrand factor.

the lung tissues on day 1 (data not shown). Importantly, plasma samples from mice injected with mock-transfected PC-9$^{ffLuc\text{-}cp156}$ cells showed decreased amount of large VWF multimers compared with mice injected with or without ADAM28-shRNA transfectants (n = 3 mice per each group) (Figure 6, G).

Intravenous administrations of ADAM28-siRNA on days 3, 6, and 9, after PC-9$^{ffLuc\text{-}cp156}$ cell injection, showed statistically significantly reduced lung metastasis at week 2 and week 3 (mean photon counts in non-silencing siRNA [n = 9 mice] vs ADAM28 siRNA [n = 9 mice] at week 3: 217 × 10^6 vs 36 × 10^6 photons/s, difference = 181 × 10^6 photons/s, 95% CI = 161 × 10^6 to 201 × 10^6 photons/s, $P < .001$) (Figure 7, A). Furthermore, PC-9$^{ffLuc\text{-}cp156}$ cells that were pretreated with neutralizing anti-ADAM28 antibody showed statistically significantly reduced lung metastasis compared with those pretreated with non-immune IgG (mean photon counts in non-immune IgG [n = 9 mice] vs anti-ADAM28 antibody [n = 9 mice] treatment at week 2: 243 × 10^6 vs 102 × 10^6 photons/s, difference = 141 × 10^6 photons/s, 95% CI = 87 × 10^6 to 195 × 10^6 photons/s, $P = .003$) (Figure 7, B).

Effect of ADAM28 Knockdown on Primary Tumor Growth and Spontaneous Metastasis

Primary tumor growth and spontaneous metastasis were compared by orthotopic injection of mock- and ADAM28-shRNA transfectants of MDA-MB231$^{ffLuc\text{-}cp156}$ cells into mammary fat pads of NOD/SCID mice (n = 10 mice per group). Between week 3 and week 6 after cell injection, the primary tumor growth of ADAM28-shRNA transfectants was statistically significantly reduced compared with mock-transfectants (mean photon counts in mock [n = 10 mice] vs shADAM28 [n = 10 mice] at week 6: 432 × 10^6 vs 120 × 10^6 photons/s, difference = 312 × 10^6 photons/s, 95% CI = 263 × 10^6 to 361 ×10^6 photons/s, $P < .001$) (Figure 8, A), confirming our previous data observed with ADAM28-siRNA (13). RT-PCR analysis for the expression of ffLuc-cp156 transcripts in the lung, heart, liver, kidney, and brain from mice (n = 10 mice per group) at week 6 indicated a reduction in the overall metastasis of ADAM28-shRNA transfectants compared with mock-transfectants (Figure 8, B). In all organs analyzed, inhibition of ADAM28 expression showed substantial inhibition of metastasis, indicated by decreased level of expression of ffLuc-cp156 transcripts (percentage of metastasis-positive sample number to total number, mock vs shADAM28: lungs, 50% vs 10%; heart, 20% vs 10%; liver, 70% vs 30%; kidneys, 70% vs 20%; and brain, 20% vs 0%). Similar suppressive effect of ADAM28-shRNA transfectants (n = 5 mice) vs mock transfectants (n = 5 mice) of PC-9$^{ffLuc\text{-}cp156}$ cells on primary tumor growth was obtained, but no metastases were detected by RT-PCR in either transfectants (data not shown).

Discussion

In this study, we used the yeast two-hybrid system and screened the human lung cDNA library to identify new substrates of

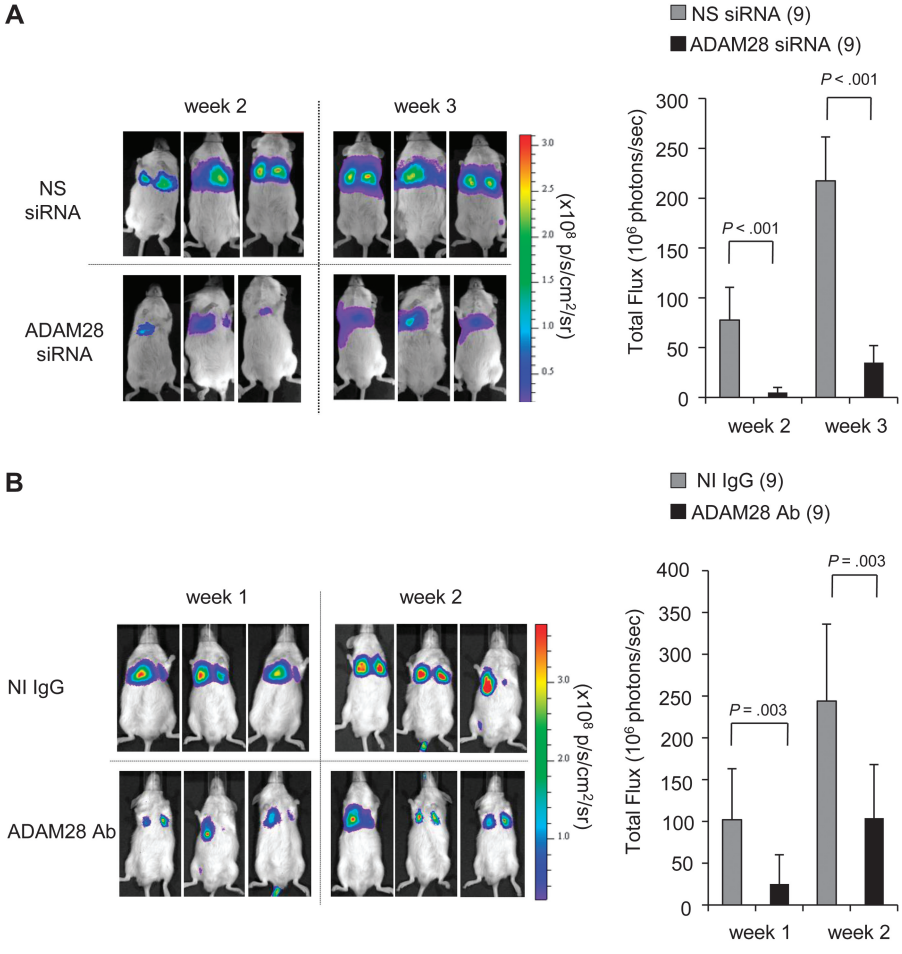

Figure 7. Knockdown of ADAM28 expression using small interfering RNA (siRNA) or inhibition of activity using ADAM28-specific antibody and effect on lung metastasis. **A**) Bioluminescence imaging of mice treated with atelocollagen-mediated ADAM28 siRNA. Nonobese diabetic/severe combined immunodeficient mice were intravenously injected with ADAM28 siRNA or non-silencing siRNA (NS siRNA) in atelocollagen on days 3, 6, and 9 after giving them intravenous injection of PC-9$^{ffLuc\text{-}cp156}$ cells, and lung metastasis was determined by bioluminescence imaging at week 2 and week 3 after PC-9$^{ffLuc\text{-}cp156}$ cell injection. Mean values and upper 95% confidence intervals from three independent experiments with three mice per group are shown in the **bar graph**. The total number of mice in each group is shown in **parentheses**. **B**) Bioluminescence imaging of mice intravenously injected with PC-9$^{ffLuc\text{-}cp156}$ cells incubated with 5 μg/mL anti-human ADAM28 mouse monoclonal antibody (ADAM28 Ab) or 5 μg/mL nonimmune (NI) IgG before injection. Lung metastasis was determined by bioluminescence imaging at week 1 and week 2 after intravenous injection. Mean values and upper 95% confidence intervals from three independent experiments with three mice per group are shown in the **bar graph**. The total number of mice in each group is shown in **parentheses**. ADAM28 = a disintegrin and metalloproteinase 28.

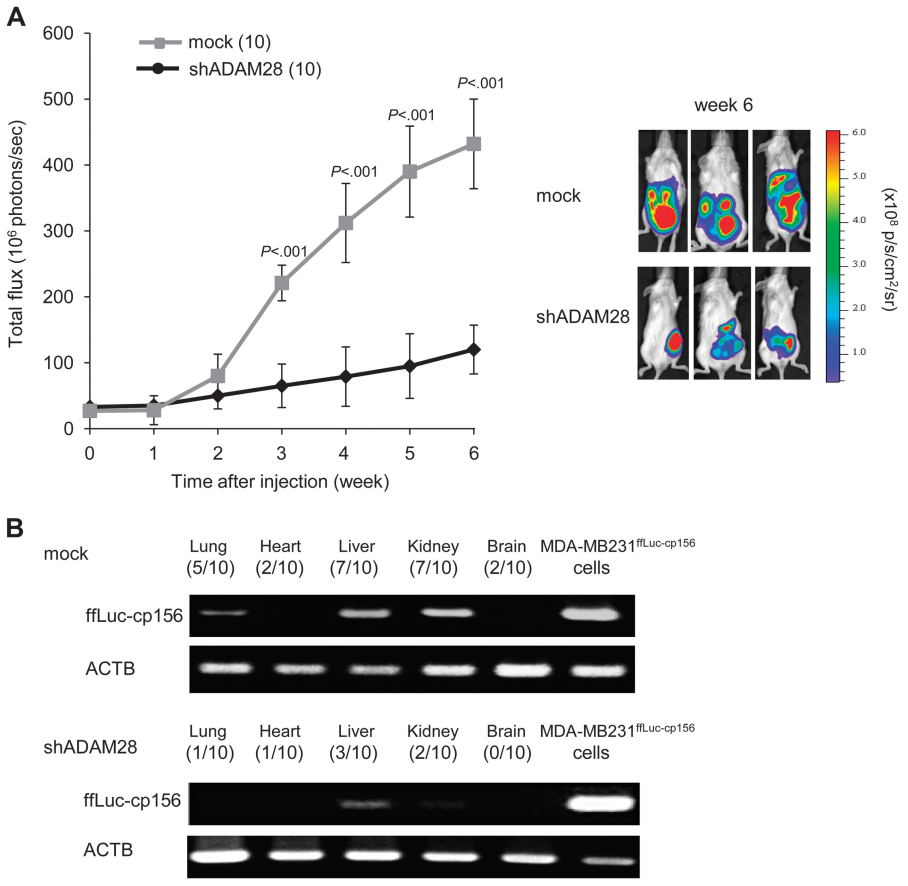

Figure 8. Knockdown of ADAM28 in MDA-MB231$^{ffLuc\text{-}cp156}$ cells using short hairpin RNA (shRNA) and effect on primary tumor growth and spontaneous organ metastasis. **A**) Primary tumor growth. MDA-MB231$^{ffLuc\text{-}cp156}$ cells (2×10^6) stably transfected with lentiviral vectors of shRNA for ADAM28 (shADAM28) or mock vectors (mock) were orthotopically injected into mammary fat pads of nonobese diabetic/severe combined immunodeficient (NOD/SCID) mice. Tumor growth was monitored weekly for 6 weeks by bioluminescence imaging (left panel). Data shown are mean values and upper 95% confidence intervals from two independent experiments with five mice per group. The total number of mice in each group is shown in **parentheses**. Right panel shows representative photos of bioluminescence imaging of mice at week 6 after injection of mock- and shADAM28-transfectants into mammary fat pads. *P* values were calculated using two-sided Student's *t* test. **B**) Analysis of spontaneous metastasis to distant organs. Total mRNA was extracted from the lung, heart, liver, kidney, and brain, which were isolated from NOD/SCID mice at week 6 after injection with MDA-MB231$^{ffLuc\text{-}cp156}$ cells transfected with mock or shADAM28. Reverse transcription–polymerase chain reaction analysis of ffLuc-cp156 transcripts was performed to assess metastasis in these organs. Results from two independent experiments with five mice per group are shown; **numbers in parentheses** indicate positive sample number/total number. MDA-MB231$^{ffLuc\text{-}cp156}$ cells were used as a positive control and ACTB as a loading control. ACTB = beta-actin; ADAM28 = a disintegrin and metalloproteinase 28.

ADAM28 and found that ADAM28 could bind to and cleave native VWF. We showed that human carcinoma cell lines with high-level expression of ADAM28 were resistant to VWF-induced apoptosis, but apoptosis was induced when the expression or activity was blocked using siRNA or neutralizing anti-ADAM28 antibody or in carcinoma cell lines with very low-level expression of ADAM28. These data are, to the best of our knowledge, the first evidence that ADAM28 cleaves VWF and the VWF digestion prevents VWF-induced apoptosis in human carcinoma cells in vitro. Results from the in vivo experimental model of lung metastasis in mice demonstrated that knockdown of ADAM28 expression by shRNA and siRNA or blocking of the activity using anti-ADAM28 antibody statistically significantly reduced lung metastasis. Decreased lung metastasis of ADAM28-shRNA transfectants was associated with enhanced apoptosis mainly within blood vessels and reduced VWF degradation in blood samples. Furthermore, we showed that in orthotopic implantation model of breast carcinoma in mice, shRNA-driven knockdown of ADAM28 expression suppressed spontaneous metastasis to distant organs as well as primary tumor growth.

We first identified VWF as an ADAM28-binding protein by the yeast two-hybrid system and then confirmed the interaction by the binding assay. Importantly, ADAM28 could cleave both native and denatured VWF, indicating that it has different substrate recognition specificity than the previously reported VWF-cleaving protease, ADAMTS13, which digests the single Tyr^{1605}-Met^{1606} bond within the A2 domain of VWF only under the denaturing conditions or the high shear flow stress (25,26). Because unfolding of VWF and exposure of the cryptic Tyr^{1605}-Met^{1606} site are a prerequisite to the cleavage by ADAMTS13, the action of this enzyme in circulation is primarily dependent on shear stress–induced unfolding of VWF molecule (34). Leukocyte proteinases including elastase, cathepsin G, MMP-9 and proteinase 3 are also known to clip VWF at or near the Tyr^{1605}-Met^{1606} bond under similar conditions (35). VWF is composed of the subunits designated as A to D domains (D′-D3-A1-A2-A3-D4-B1-B2-B3-C1-C2-CK) (Figure 2, D) and the D′-D3 domain is in close proximity with A1 domain (36), shielding the A1 domain from the interaction with other molecules. In contrast to the A2-domain-attacking proteinases, ADAM28 cleaves the linker regions between D3 and A1 domains and between A1 and A2 domains. Thus, it is likely that the cleavage sites are exposed in the ternary arrangement, being susceptible to ADAM28. The metalloproteinase domain of ADAM28 is known to have the highest homology to that of snake venom metalloproteinases (37). In fact, one cleavage site (the Leu^{1242}–Leu^{1243} bond) by ADAM28 was identical to the attacking site by snake venom metalloproteinase jararhagin (38). ADAMTS13 plays a physiological role in preventing inappropriate thrombus formation by proteolytic modulation of the ultralarge multimers via the unfolding of VWF by shear flow stress (39,40). Because ADAM28 lacks this regulation mechanism, like snake venom metalloproteinases, ADAM28 may be involved in the degradation of VWF under pathological, rather than physiological, conditions.

VWF is believed to function as a multimeric glue molecule to initiate adherence and aggregation of platelets to the sites of injured vessel walls, contributing essentially to the primary hemostasis. However, Terraube et al. (30) have reported a link between VWF and cancer metastasis. They showed that lung metastasis is increased in VWF-deficient mice after intravenous injection of mouse B16BL6 melanoma and Lewis lung carcinoma cells (30) and that incubation of B16BL6 cells with VWF enhances apoptosis (28). Although they did not study the effects of VWF on human carcinoma cell lines or involvement of ADAM28 in this process, our data in this study have demonstrated that VWF induces apoptosis in many human cell lines established from carcinomas of the lung, breast, kidney, and liver only when they have very low-level expression of ADAM28 or when the activity and/or expression are knocked down. These data suggest that VWF is an inducer of apoptosis in both human and mouse cancer cells and that ADAM28 negatively regulates the apoptosis through digestion of VWF.

VWF is reported to interact with tumor cells and endothelial cells through αvβ3 integrin (29,30), whereas VWF binds to αIIbβ3 integrin in platelets (41). Indeed, we have demonstrated that both PC-9 and MDA-MB231 cells express αvβ3 integrin and that apoptosis signal is transduced through this integrin. The αvβ3 integrin plays a complex role in angiogenesis and tumor growth (42). Although original data on αvβ3 integrin suggested proangiogenic and tumor growth–promoting effects (43,44), more recent studies have indicated anti-angiogenic and tumor suppressive roles (45). Accumulated lines of evidence have provided an explanation about the contradictory effects of αvβ3 on endothelial cells and tumor cells; when ligands are absent or only soluble fragments from endogenous extracellular matrix (eg, canstatin and tumstatin) or therapeutic antagonists (eg, resveratrol) are present, αvβ3 integrin activates a death pathway, resulting in suppression of angiogenesis and tumor growth (46). On the other hand, when αvβ3 integrin is ligated by immobilized extracellular matrix (eg, fibronectin and vitronectin), the mechanical anchorage to the extracellular matrix triggers survival signal (46,47). Previous study on the breast carcinoma cell lines of MCF-7 and MDA-MB231 indicated that binding of resveratrol and canstatin to αvβ3 integrin induces apoptosis through phosphorylation of TP53 (32) and activation of mitochondrial apoptotic pathway including CASP3 (33). In this study, we have demonstrated that both intracellular signaling pathways via binding to αvβ3 integrin are involved in VWF-induced apoptosis in cancer cells that were treated with soluble VWF in culture media. The concentration of VWF in normal serum is approximately 10 μg/mL (48), which is within the range of the apoptosis-inducing concentration (>3 μg/mL) used in this study. Altogether, these data suggest that VWF-induced apoptosis of human carcinoma cells depends, at least in part, on the VWF/αvβ3 integrin–mediated cell death pathway. Although beyond the scope of this study, the possibility of transdominant inhibition of cell growth–promoting integrins and/or cross-talk between integrins and growth factor receptors (47) should be clarified by future studies.

Metastasis is an inefficient process: Only 0.01%–0.02% of melanoma cells form progressively growing metastasis in the liver or lung after the intravenous injection in mice (49,50). In the lung metastasis model, an important determinant of metastatic inefficiency appears to be tumor cell apoptosis, which is prominently observed within the lungs at 24–48 hours after intravenous injection to tail vein (51). In this study, we have demonstrated that shRNA- or siRNA-driven knockdown of ADAM28 expression or inhibition of ADAM28 activity by neutralizing antibody results in statistically significantly decreased lung metastasis, which was associated with increased apoptosis of carcinoma cells within the lung blood vessels. Because VWF is a highly conserved protein among animal species, showing 91% homology between mouse and human VWF in the whole amino acid sequence and almost identical in the linker regions between D3 and A1 domains (100% homology) and between A1 and A2 domains (99% homology), it is plausible that human ADAM28 produced by carcinoma cells can digest mouse VWF in the lung tissues. Actually, our data in this study showed a decrease in VWF multimers in plasma from the mice received intravenous injection of PC-9$^{ffLuc\text{-}cp156}$ cells, suggesting the cleavage of mouse VWF by ADAM28 derived from human carcinoma cells within the lung blood vessels. Based on these findings, we propose the hypothesis that the ADAM28-dependent cleavage of VWF enhances survival of carcinoma cells in the lung blood vessels and consequently facilitates their metastases.

A potential limitation of this study was the use of the lung metastasis model as a clinically relevant model. This model does not reflect the spontaneous metastatic processes, which involve continuous and persistent intravasation of invading carcinoma cells from the primary tumors. Therefore, we carried out the experiments by orthotopic injection of MDA-MB231$^{ffLuc\text{-}cp156}$ cells into mouse mammary fat pads and found that ADAM28 knockdown reduces both primary tumor growth and spontaneous metastasis. The researchers were not blinded to the groups, and therefore this bears the risk of biased interpretation. Nevertheless, the results suggest that ADAM28 has dual promoting effects on carcinoma cell proliferation and spontaneous metastasis to distant organs. The enhanced primary tumor growth may be explained by increased bioavailability of IGF-I through IGFBP-3 digestion of the IGF-I/IGFBP-3 complex by ADAM28, as we reported previously (13). Although it is possible to speculate that the promoting effect of ADAM28 on spontaneous metastasis is because of enhanced survival of carcinoma cells by escaping from VWF-induced apoptosis after their intravasation, we cannot exclude the possibility that this is partly because of higher frequency of vascular invasion by carcinoma cells in the substantially larger primary tumors. Therefore, further studies are still needed to determine the role of ADAM28-mediated VWF digestion in spontaneous metastasis.

The experimental data in this study showing successful inhibition of lung metastasis and spontaneous metastasis as well as primary tumor growth by targeting ADAM28 using shRNA, siRNA, or anti-ADAM28 antibody suggest the possibility that ADAM28 can be a molecular target in the patients with non–small cell lung carcinoma or breast carcinoma. Therefore, measurement of ADAM28 protein in the primary carcinoma tissues and/or blood samples from patients with the carcinoma can be a useful method for prediction of metastasis. In addition, the development of inhibitors selective or specific to ADAM28 including synthetic peptide inhibitors or monoclonal antibodies is expected, and deliberate and detailed analyses of the function of ADAM28 in both physiological

and diseased conditions are needed in order for the inhibitors to be applied in future clinical trials.

References

1. Edwards DR, Handsley MM, Pennington CJ. The ADAM metalloproteinases. *Mol Aspects Med.* 2008;29(5):258–289.
2. Murphy G. Regulation of the proteolytic disintegrin metalloproteinases, the 'Sheddases'. *Semin Cell Dev Biol.* 2009;20(2):138–145.
3. Shiomi T, Lemaitre V, D'Armiento J, Okada Y. Matrix metalloproteinases, a disintegrin and metalloproteinases, and a disintegrin and metalloproteinases with thrombospondin motifs in non-neoplastic diseases. *Pathol Int.* 2010;60(7):477–496.
4. Seals DF, Courtneidge SA. The ADAMs family of metalloproteases: multidomain proteins with multiple functions. *Genes Dev.* 2003;17(1):7–30.
5. Mochizuki S, Okada Y. ADAMs in cancer cell proliferation and progression. *Cancer Sci.* 2007;98(5):621–628.
6. Blobel CP. ADAMs: key components in EGFR signalling and development. *Nat Rev Mol Cell Biol.* 2005;6(1):32–43.
7. Okada Y. Proteinases and matrix degradation. In: Firestein GS BRC, Harris ED Jr., McInnes IB, Ruddy S, Sargent JS, eds. *Kelley's Textbook of Rheumatology.* 8th ed. Philadelphia, PA: Elsevier Saunders; 2009:115–134.
8. White JM. ADAMs: modulators of cell-cell and cell-matrix interactions. *Curr Opin Cell Biol.* 2003;15(5):598–606.
9. Murphy G. The ADAMs: signalling scissors in the tumour microenvironment. *Nat Rev Cancer.* 2008;8(12):929–941.
10. Roberts CM, Tani PH, Bridges LC, Laszik Z, Bowditch RD. MDC-L, a novel metalloprotease disintegrin cysteine-rich protein family member expressed by human lymphocytes. *J Biol Chem.* 1999;274(41):29251–29259.
11. Mochizuki S, Okada Y. ADAM28 as a target for human cancers. *Curr Pharm Des.* 2009;15(20):2349–2358.
12. Ohtsuka T, Shiomi T, Shimoda M, et al. ADAM28 is overexpressed in human non-small cell lung carcinomas and correlates with cell proliferation and lymph node metastasis. *Int J Cancer.* 2006;118(2):263–273.
13. Mitsui Y, Mochizuki S, Kodama T, et al. ADAM28 is overexpressed in human breast carcinomas: implications for carcinoma cell proliferation through cleavage of insulin-like growth factor binding protein-3. *Cancer Res.* 2006;66(20):9913–9920.
14. Kuroda H, Mochizuki S, Shimoda M, et al. ADAM28 is a serological and histochemical marker for non-small-cell lung cancers. *Int J Cancer.* 2010; 127(8):1844–1856.
15. Mochizuki S, Tanaka R, Shimoda M, et al. Connective tissue growth factor is a substrate of ADAM28. *Biochem Biophys Res Commun.* 2010; 402(4):651–657.
16. Shimoda M, Hashimoto G, Mochizuki S, et al. Binding of ADAM28 to P-selectin glycoprotein ligand-1 enhances P-selectin-mediated leukocyte adhesion to endothelial cells. *J Biol Chem.* 2007;282(35):25864–25874.
17. Hashimoto G, Shimoda M, Okada Y. ADAMTS4 (aggrecanase-1) interaction with the C-terminal domain of fibronectin inhibits proteolysis of aggrecan. *J Biol Chem.* 2004;279(31):32483–32491.
18. Soejima K, Mimura N, Hirashima M, et al. A novel human metalloprotease synthesized in the liver and secreted into the blood: possibly, the von Willebrand factor-cleaving protease? *J Biochem.* 2001;130(4):475–480.
19. Mochizuki S, Shimoda M, Shiomi T, Fujii Y, Okada Y. ADAM28 is activated by MMP-7 (matrilysin-1) and cleaves insulin-like growth factor binding protein-3. *Biochem Biophys Res Commun.* 2004;315(1):79–84.
20. Soejima K, Nakamura H, Hirashima M, Morikawa W, Nozaki C, Nakagaki T. Analysis on the molecular species and concentration of circulating ADAMTS13 in blood. *J Biochem.* 2006;139(1):147–154.
21. Asakura M, Kitakaze M, Takashima S, et al. Cardiac hypertrophy is inhibited by antagonism of ADAM12 processing of HB-EGF: metalloproteinase inhibitors as a new therapy. *Nat Med.* 2002;8(1):35–40.
22. Hara-Miyauchi C, Tsuji O, Hanyu A, et al. Bioluminescent system for dynamic imaging of cell and animal behavior. *Biochem Biophys Res Commun.* 2012;419(2):188–193.
23. Hayashi I, Tome Y, Shimosato Y. Thiosemicarbazide used after periodic acid makes methenamine silver staining of renal glomerular basement membranes faster and cleaner. *Stain Technol.* 1989;64(4):185–190.
24. Soejima K, Matsumoto M, Kokame K, et al. ADAMTS-13 cysteine-rich/spacer domains are functionally essential for von Willebrand factor cleavage. *Blood.* 2003;102(9):3232–3237.
25. Furlan M, Robles R, Lammle B. Partial purification and characterization of a protease from human plasma cleaving von Willebrand factor to fragments produced by in vivo proteolysis. *Blood.* 1996;87(10):4223–4234.
26. Tsai HM. Physiologic cleavage of von Willebrand factor by a plasma protease is dependent on its conformation and requires calcium ion. *Blood.* 1996;87(10):4235–4244.
27. Mancuso DJ, Tuley EA, Westfield LA, et al. Structure of the gene for human von Willebrand factor. *J Biol Chem.* 1989;264(33):19514–19527.
28. Terraube V, Marx I, Denis CV. Role of von Willebrand factor in tumor metastasis. *Thromb Res.* 2007;120(suppl 2):S64–S70.
29. Pilch J, Habermann R, Felding-Habermann B. Unique ability of integrin alpha(v)beta 3 to support tumor cell arrest under dynamic flow conditions. *J Biol Chem.* 2002;277(24):21930–21938.
30. Terraube V, Pendu R, Baruch D, et al. Increased metastatic potential of tumor cells in von Willebrand factor-deficient mice. *J Thromb Haemost.* 2006;4(3):519–526.
31. Floyd CM, Irani K, Kind PD, Kessler CM. von Willebrand factor interacts with malignant hematopoietic cell lines: evidence for the presence of specific binding sites and modification of von Willebrand factor structure and function. *J Lab Clin Med.* 1992;119(5):467–476.
32. Lin HY, Lansing L, Merillon JM, et al. Integrin alphaVbeta3 contains a receptor site for resveratrol. *FASEB J.* 2006;20(10):1742–1744.
33. Magnon C, Galaup A, Mullan B, et al. Canstatin acts on endothelial and tumor cells via mitochondrial damage initiated through interaction with alphavbeta3 and alphavbeta5 integrins. *Cancer Res.* 2005;65(10): 4353–4361.
34. Zhang Q, Zhou YF, Zhang CZ, Zhang X, Lu C, Springer TA. Structural specializations of A2, a force-sensing domain in the ultralarge vascular protein von Willebrand factor. *Proc Natl Acad Sci U S A.* 2009;106(23): 9226–9231.
35. Raife TJ, Cao W, Atkinson BS, et al. Leukocyte proteases cleave von Willebrand factor at or near the ADAMTS13 cleavage site. *Blood.* 2009;114(8):1666–1674.
36. Ulrichts H, Udvardy MS, Lenting PJ, et al. Shielding of the A1 domain by the D ' D3 domains of von Willebrand factor modulates its interaction with platelet glycoprotein Ib-IX-V. *J Biol Chem.* 2006;281(8): 4699–4707.
37. Igarashi T, Araki S, Mori H, Takeda S. Crystal structures of catrocollastatin/VAP2B reveal a dynamic, modular architecture of ADAM/adamalysin/reprolysin family proteins. *FEBS Lett.* 2007;581(13): 2416–2422.
38. Serrano SMT, Wang DY, Shannon JD, Pinto AFM, Polanowska-Grabowska RK, Fox JW. Interaction of the cysteine-rich domain of snake venom metalloproteinases with the A1 domain of von Willebrand factor promotes site-specific proteolysis of von Willebrand factor and inhibition of von Willebrand factor-mediated platelet aggregation. *FEBS J.* 2007; 274(14):3611–3621.
39. Soejima K, Nakagaki T. Interplay between ADAMTS13 and von Willebrand factor in inherited and acquired thrombotic microangiopathies. *Semin Hematol.* 2005;42(1):56–62.
40. Zhang X, Halvorsen K, Zhang CZ, Wong WP, Springer TA. Mechanoenzymatic cleavage of the ultralarge vascular protein von Willebrand factor. *Science.* 2009;324(5932):1330–1334.
41. Bennett JS. Structure and function of the platelet integrin alphaIIbbeta3. *J Clin Invest.* 2005;115(12):3363–3369.
42. Desgrosellier JS, Cheresh DA. Integrins in cancer: biological implications and therapeutic opportunities. *Nat Rev Cancer.* 2010;10(1):9–22.
43. Brooks PC, Clark RA, Cheresh DA. Requirement of vascular integrin alpha v beta 3 for angiogenesis. *Science.* 1994;264(5158):569–571.
44. Brooks PC, Montgomery AM, Rosenfeld M, et al. Integrin alpha v beta 3 antagonists promote tumor regression by inducing apoptosis of angiogenic blood vessels. *Cell.* 1994;79(7):1157–1164.
45. Reynolds LE, Wyder L, Lively JC, et al. Enhanced pathological angiogenesis in mice lacking beta3 integrin or beta3 and beta5 integrins. *Nat Med.* 2002;8(1):27–34.

46. Cheresh DA, Stupack DG. Integrin-mediated death: an explanation of the integrin-knockout phenotype? *Nat Med.* 2002;8(3):193–194.
47. Hynes RO. A reevaluation of integrins as regulators of angiogenesis. *Nat Med.* 2002;8(9):918–921.
48. Sadler JE. Biochemistry and genetics of von Willebrand factor. *Annu Rev Biochem.* 1998;67:395–424.
49. Chambers AF, Groom AC, MacDonald IC. Dissemination and growth of cancer cells in metastatic sites. *Nat Rev Cancer.* 2002;2(8):563–572.
50. Talmadge JE, Fidler IJ. AACR centennial series: the biology of cancer metastasis: historical perspective. *Cancer Res.* 2010;70(14):5649–5669.
51. Wong CW, Lee A, Shientag L, et al. Apoptosis: an early event in metastatic inefficiency. *Cancer Res.* 2001;61(1):333–338.

Funding

This work was supported by Grant-in-Aid for Scientific Research (C) from the Ministry of Education, Culture, Sports, Science and Technology of Japan (MEXT) (to SM), Grant-in-Aid for Scientific Research (S) (19109004) and Grant-in-Aid for Scientific Research (A) (24249022) from MEXT, Third Term 10-year Strategy for Cancer Control from the Ministry of Health and Welfare (to YO), and Grant-in-Aid for the Global COE program from MEXT (to Keio University).

Notes

We thank Ms Aya Shiraishi for her technical assistance and Dr Shuji Yamashita for his useful advice on immunohistochemistry. We are grateful to Dr Tomoko Betsuyaku and Dr Mitsuyasu Kato for their advice and support in the experiments using non-neoplastic cell lines, and Dr Ken Ishii and Dr Yumi Matsuzaki for helping us with the In Vivo Imaging System (IVIS) system and MoFlo flow cytometer, respectively. The authors are solely responsible for the design of the study; the collection, analysis, and interpretation of the data; the writing of the article; and the decision to submit the article for publication.

Affiliations of authors: Department of Pathology (SM, MS, HA, AS, YO) and Department of Physiology (HJO, HO), School of Medicine, Keio University, Tokyo, Japan; First Research Department, The Chemo-Sero-Therapeutic Research Institute, Kumamoto, Japan (KS); RIKEN Keio University Joint Research Laboratory, Brain Science Institute, RIKEN, Saitama, Japan (HO).